Formation and temperature dependence of Highly Oxygenated Organic Molecules (HOM) from Δ^3-carene ozonolysis

Yuanyuan Luo[1*], Ditte Thomsen[2], Emil Mark Iversen[2], Pontus Roldin[3,4], Jane Tygesen Skønager[2], Linjie Li[5], Michael Priestley[5], Henrik B. Pedersen[6], Mattias Hallquist[5], Merete Bilde[2], Marianne Glasius[2], and Mikael Ehn[1*]

[1]Institute for Atmospheric and Earth System Research (INAR), University of Helsinki, Helsinki, 000149, Finland
[2]Department of Chemistry, Aarhus University, Aarhus C, 8000, Denmark
[3]Department of Physics, Lund University, Lund, 22100, Sweden
[4]IVL, Swedish Environmental Research Institute, SE-211 19 Malmö, Sweden
[5]Department of Chemistry and Molecular Biology, University of Gothenburg, Gothenburg, 41296, Sweden
[6]Department of Physics and Astronomy, Aarhus University, Aarhus C, 8000, Denmark

Correspondence to: Yuanyuan Luo (yuanyuan.luo@helsinki.fi) and Mikael Ehn (mikael.ehn@helsinki.fi)

This file contains:

1: Details for chamber facilities;
2: HOM dynamics and yield estimates;
Figures S1-S14
Tables S1-S7

1. Details for chamber facilities

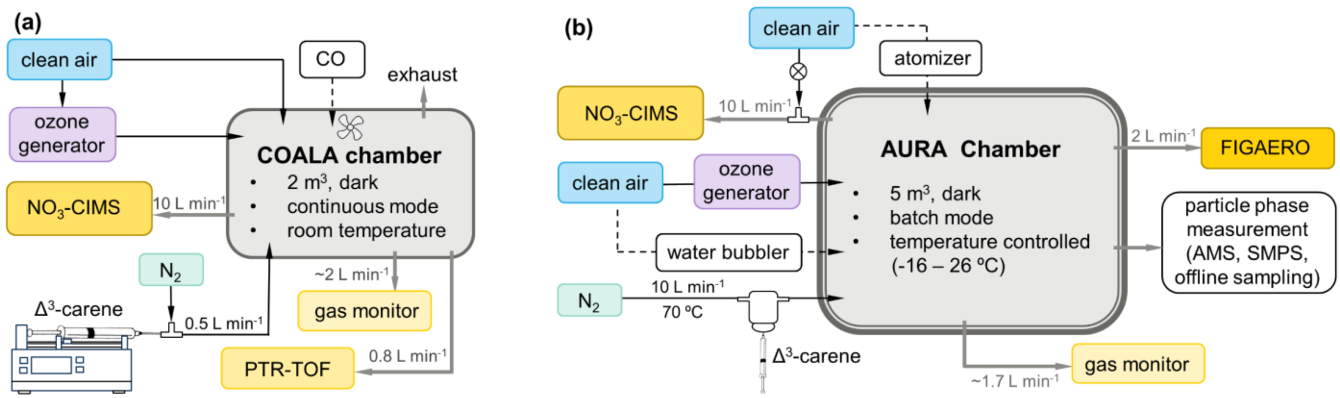

Figure S1. Experiment set-ups. The set-up of experiments conducted in the COALA chamber is shown in panel (a), while the set-up in AURA chamber is shown in panel (b). The dashed lines represent the injection only used for specific experiments.

COALA chamber

The COALA chamber is a 2 m^3 Teflon reactor, which is maintained at room temperature (25 ± 1℃) and under dry conditions with RH < 1%. To prevent contamination from external sources, the chamber was operated at a slightly elevated pressure (~3 Pa). More details of the COALA chamber can be found in Riva et al. (2019). During this campaign, the chamber was run in continuous mode with a total inflow of 40 L min^{-1} (average residence time: ~ 50 min). Each experiment ran for a minimum of 140 minutes, allowing the chamber to reach a steady state. For a more in-depth discussion about the dynamics of our continuous mode "steady-state" chamber, see Peräkylä et al. (2020). Purified dry air was injected into the chamber as the main inflow, while ozone was generated and injected by passing 5 L min^{-1} purified air through a Dasibi 1008-PC ozone generator. Δ^3-carene or α-pinene (for comparison) was introduced using a syringe pump with a 0.5 L min^{-1} nitrogen flow as the carrier gas. The injection rate of VOC or the strength of the ozone generator was adjusted to achieve different oxidation conditions in the chamber. In some experiments (Table S1), approximately 200 ppm of CO from a gas bottle was introduced to the chamber as an OH scavenger. The majority of the outflow from the chamber was sampled by instruments, while the remaining flow was flushed out as exhaust. A schematic of the COALA chamber setup is shown in Figure S1(a).

Measurements of temperature, RH, and pressure inside the chamber were obtained using a Vaisala temperature and humidity probe (INTERCAP® HMP60), and a differential pressure sensor (Sensirion SDP1000-L025). To monitor the precursors and oxidation products of Δ^3-carene ozonolysis, two state-of-the-art mass spectrometers were utilized. A proton transfer reaction time-of-flight mass spectrometer (PTR-TOF 8000, Ionicon Analytik Gmbh) was deployed to measure VOC concentrations, calibrated before the experiments directly with a mixture of VOCs, including monoterpenes. A chemical ionization atmospheric pressure interface time-of-flight mass analyser (CIMS, Tofwerk AG/Aerodyne Research, Inc.) was employed to probe oxygenated products from Δ^3-carene ozonolysis, with a primary focus on HOM. Nitric acid (HNO_3) and an X-ray source were used to produce nitrate reagent ions (NO_3^-) for the CI inlet. The equipped long TOF analyser enables the measurement of ions within the HOM region (m/z 300 – 600 Th) with a mass resolving power of ~8000 Th. During the experiments, the NO_3-CIMS continuously sampled chamber flow at a rate of 10 L min^{-1} and recorded averaged mass spectra every 10 s. The data from both PTR-TOF and NO_3-CIMS were pre-processed using the tofTools MATLAB package (version 612). Chamber background was determined during the period before VOC injection in each experiment. All data collected in the COALA chamber, unless specified otherwise, were subtracted with chamber background and averaged to 10 min resolution. Further technical details and instrument specifications have been presented by Jordan et al. (2009) and Jokinen et al. (2012) for PTR-TOF and NO_3-CIMS, respectively.

Table S1. Experimental conditions for Δ^3-carene (a) and α-pinene (b) ozonolysis conducted in the COALA chamber. For all experiments, the chamber was run in continuous mode at room temperature (25 ± 1°C) and dry conditions (RH < 1%).

(a)	Date	Experiment	injected Δ^3-carene (ppb)	injected O_3 (ppb)	injected CO (ppm)
	2023-2-9	1	10±1	30±2	
		2	20±2	30±2	
		3	20±2	30±2	~200
		4	30±2	30±2	~200
		5	30±2	30±2	
	2023-2-10	6	10±1	30±2	
		7	30±2	30±2	
		8	30±2	50±3	
	2023-2-11*	9	30→0	30±2	
	2023-2-13	10	20±2	30±2	
	2023-2-14	11	20±2	30±2	~200

(b)	Date	Experiment	injected α-pinene (ppb)	injected O_3 (ppb)	injected CO (ppm)
	2023-2-6	12	20±2	30±2	
		13	25±1	45±1	
	2023-2-7	14	50±2	60±1	
		15	50±2	60±1	
	2023-2-8	16	45±2	13±1	
		17	45±2	13±1	~200
		18	45±2	13±1	
	2023-2-14	19	20±2	30±2	
		20	20±2	30±2	~200

* The Δ^3-carene in the syringe ran out at around 10:40 am, resulting in the injection of Δ^3-carene decreased from ~30 ppb to 0 ppb gradually afterwards.

AURA chamber

Table S2. Experimental conditions for Δ^3-carene ozonolysis experiments conducted in the AURA chamber. Carene and O_3 are the starting concentrations of VOC and O_3 at experiment time=0 min, respectively.

						NO3-CIMS condition	
Date	Experiment	Δ^3-carene (ppb)	O_3 (ppb)	T (°C)	RH (%)	flow from chamber* (L min^{-1})	Setting#
2022-1-11	20A	10±5	181±15	20.2±0.1	0±0	5	1
2022-1-13	10A	10±5	174±15	10.1±0.1	0±0	5	1
2022-1-24	10D	10±5	174±15	10.2±0.1	78±2	10	2
2022-1-31	10E	20±5	169±15	10.2±0.1	76±1	10	2
2022-2-2	0A	10±5	159±15	0.1±0.1	1.6±1.6	10	3
2022-2-4	10B	10±5	171±15	10.1±0.1	0.4±0.8	10	3
2022-2-5	20B	10±5	181±15	20.2±0.1	0±0	10	3

* The total inlet flow of NO_3-CIMS was 10 L min^{-1} for all experiments, and the flow from chamber shows the proportion of the total inlet flow sampled directly from the chamber.

During the AURA chamber campaign, the setting of NO_3-CIMS was modified three times. Setting 1 was the original settings. In Setting 2, the TofDaq setting was kept the same as in Setting 1, but the TPS setting was adjusted. In Setting 3, the TPS settings remained the same as in Setting 2, while the ToFDaq setting was altered. By rapidly switching between Setting 2 and 3 at some point during the experiments, a correction factor of 2.43 was determined for Setting 2 to enable comparability of the data collected using this setting with that obtained using Setting 3.

The AURA chamber is a 5 m^3 Teflon chamber situated in a temperature-controlled room (temperature range: -16 – 26 °C). A detailed description of the AURA chamber can be found in Kristensen et al. (2017).The setup of the AURA chamber is illustrated in Figure S1(b). Throughout the campaign, the AURA chamber was run in batch mode, meaning the sources and sinks for products were progressively accumulated from the beginning of each experiment. For each experiment, the chamber was first filled with purified air, and a specific amount of water vapour and O_3 were injected to achieve the desired RH and O_3 levels. The experiment commenced with the introduction of 10 or 20 ppb Δ^3-carene into the chamber, marking the time as experiment time = 0 min. The conditions of the ozonolysis experiments conducted in the AURA chamber are briefly summarized in Table S2, while a comprehensive description of the experiments can be found in Thomsen et al. (2024). In general, the HOM formation of Δ^3-carene ozonolysis was examined under dry conditions (RH < 15%) at 20 °C (20A & B), 10 °C (10A & B), and 0 °C (0A), and twice under humid conditions (RH = 80%) at 10 °C with two different Δ^3-carene loadings (10D: 10 ppb and 10 E: 20 ppb).

As shown in Figure S1(b), instruments for both gas phase and particle phase measurements were utilized. Particle size distributions were determined using a scanning mobility particle sizer (SMPS, TSI Incorporated), while the chemical composition of the aerosols was analysed with a high-resolution time-of-flight aerosol mass spectrometer (AMS, Aerodyne Research, Inc., Decarlo et al. (2006)), and a filter-inlet for gases and aerosols chemical ionization mass spectrometer (FIGAERO, Lopez-Hilfiker et al. (2014)). Additionally, particles were continuously collected with a sequential spot sampler (Series 110 A, Aerosol Devices, Eiguren Fernandez et al. (2014); Eiguren-Fernandez et al. (2014)) for detailed offline analysis using an ultra-high performance liquid chromatography (UHPLC) coupled with a quadrupole time-of-flight mass spectrometry (QTOF-MS, Compact, Bruker). For HOM measurement, a NO_3-CIMS with a long TOF analyser (Tofwerk AG/Aerodyne Research, Inc.) was employed (Jokinen et al., 2012). The inlet flow rate of the NO_3-CIMS was 10 L min^{-1} for all experiments listed in Table S2. However, for 20A and 10A experiments, a dilution flow of purified air (5 L min^{-1}) was added to the sample flow from the chamber (5 L min^{-1}), while the total 10 L min^{-1} of the inlet flow was from the chamber for the remaining experiments. Due to unknown instrumental issues causing a dramatic decrease in sensitivity, certain voltage and acquisition settings of the NO_3-CIMS had to be manually adjusted during the campaign to improve the signal strengths. This adds additional uncertainties to our ability to compare different experiments. Some key parameters of the instrument in each experiment are shown in Figure S2. By rapidly switching between Setting 2 and 3 at certain points during the experiments, a correction factor of 2.43 was estimated for scaling data collected with Setting 2 to data collected with Setting 3 (Figure S3). The NO_3-CIMS data was pre-processed with the tofTools MATLAB package (version 612). Chamber background was determined during the period before VOC injection in each experiment, and all NO_3-CIMS data were after background subtraction.

This study is exclusively concentrated on the formation of HOM from Δ^3-carene ozonolysis in the gas phase. For further insights into particle phase properties and composition, detailed analyses using AMS, SMPS, and UHPLC-QTOF-MS are provided in the work of Thomsen et al. (2024). Additionally, research on the partitioning of volatile organic compounds, employing the FIGAERO, is extensively discussed in the study by Li et al. (2024).

Continuous vs. batch-mode chamber

Continuous and batch modes are commonly employed in environmental chamber studies to investigate atmospheric processes. In continuous mode, exemplified by the COALA chamber in our study, there is a constant inflow of air with steady concentrations of reactants, matched by an equal total outflow. The balance between sources and sinks allows the chamber to reach a steady state, characterized by consistent concentrations of precursors and products. The duration to achieve steady state primarily depends on the total inflow rate. In contrast, batch mode, as demonstrated by the AURA chamber in this study, involves introducing a fixed amount of reactants into a clean chamber at once. This leads to a high initial concentration of precursors that diminishes over time due to chemical reactions and physical processes, with product concentrations accumulating progressively. Batch mode, however, requires careful consideration of mixing to prevent the formation of local hot spots and ensure homogeneity. Continuous mode offers the advantage of studying reaction dynamics under stable conditions, reducing the effects of local concentration disparities and ensuring a uniform reaction environment over time, while batch mode effectively simulates abrupt atmospheric events, and allows for the examination of the aging process over longer periods.

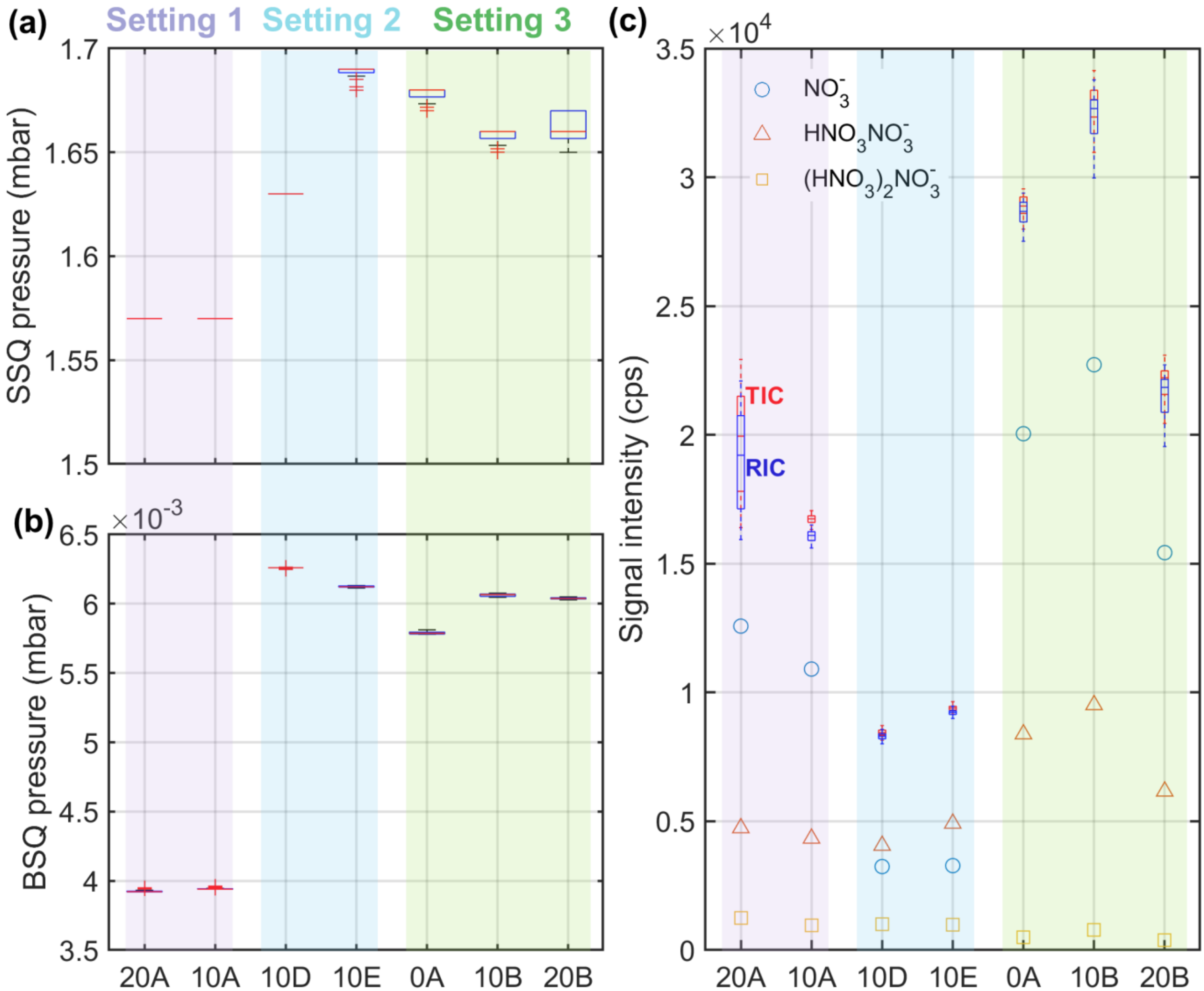

Figure S2. NO_3-CIMS pressures in the SSQ (a) and BSQ (b) chambers, and signal counts (c) of different experiments conducted in the AURA chamber. Box plots in panel (c) shows averages of the sum of all ion signals (TIC: red) and the sum of all reagent ion signals (RIC: blue). Signal intensities of reagent ions are also shown separately with different markers in panel (c). The colours of shaded areas in all panels represent different settings of NO_3-CIMS.

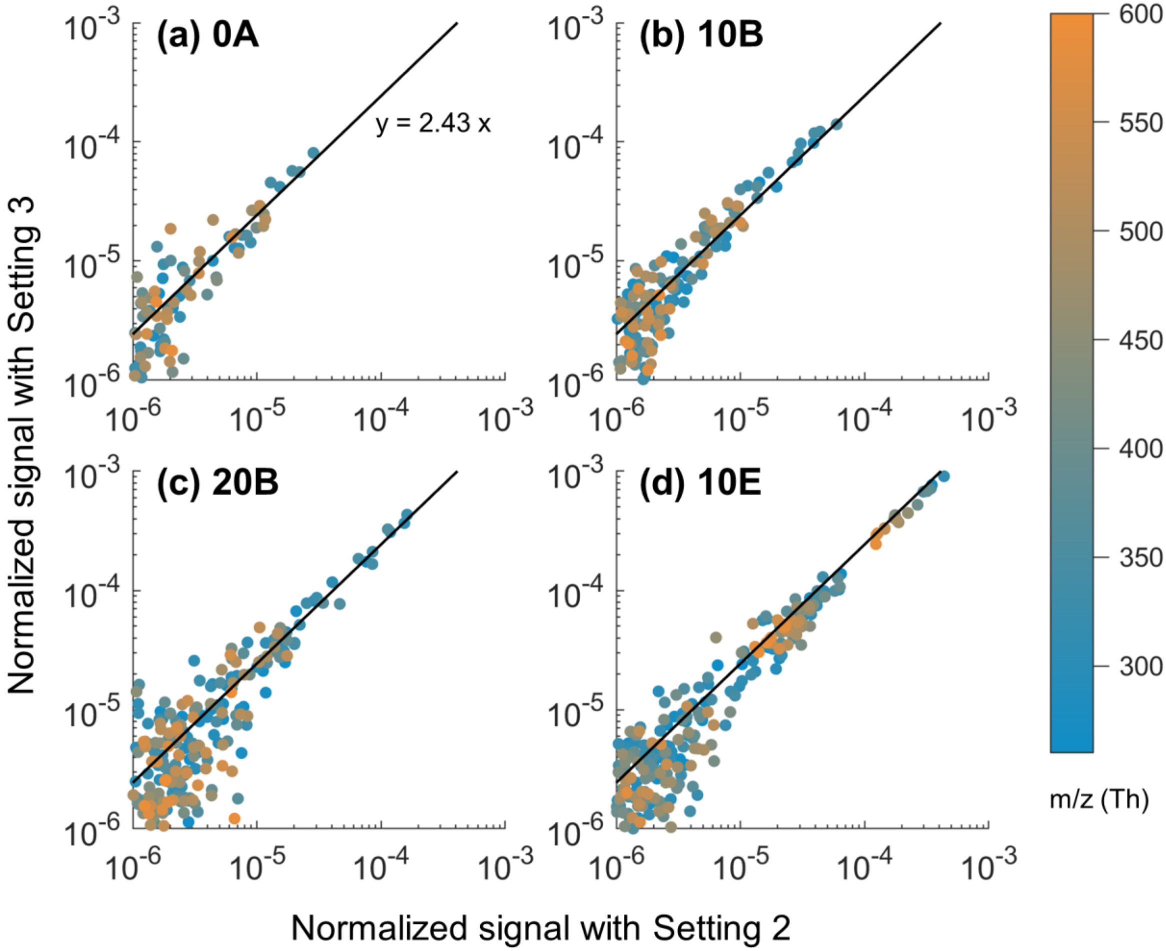

Figure S3. Scatter plot of the normalized signal intensity with Setting 2 and Setting 3. The colour shows the mass to charge ratio in the spectra where the compound was identified. The black solid lines indicates y: x=2.43. For experiments 0A, 10B, 20B and 10E in the AURA chamber, after the experiments starting for around 70-80 min, the TofDaq settings of the instrument was quickly switched to the another (Setting 3 to 2 for 0A, 10B, and 20B; Setting 3 to 2 for 10E) to collect data for 5-10 min. As the change of the products was slow at that time, the difference in the signal intensities was mainly caused by the change of the setting. We estimated a factor of 2.43 to convert the data collected with Setting 2 to Setting 3 based on the averaged slop of the linear fit.

2. HOM dynamics and yield estimates

The rate of change in HOM concentration within a chamber can be expressed as:

$$\frac{d[HOM]}{dt} = Production_{HOM} - Loss_{HOM} \quad (1)$$

Where $Production_{HOM}$ and $Loss_{HOM}$ are the total production and loss rates of HOM, respectively. [HOM] is the concentration of HOM in the chamber, which can be estimated as:

$$[HOM] = C \times \frac{\sum_i HOM_i \cdot NO_3^-}{NO_3^- + HNO_3NO_3^- + (HNO_3)_2NO_3^-} \quad (2)$$

Here C is a calibration factor ($C=1\times10^{10}$ cm^{-3} in this study). $HOM_i \cdot NO_3^-$ is the signal intensity of a cluster of a HOM specie with NO_3^-, and $(HNO_3)_jNO_3^-$ (j=0,1,2) is the signal intensity of reagent ions measured by NO_3-CIMS. Note that the NO_3-CIMS was not calibrated in this study, and therefore quantification of HOM has a very large uncertainty, estimated to be at least a factor 3. The ionization of HOM with the NO_3-CIMS is expected to be collision limited, i.e. HOM collide with NO_3^- forming clusters irreversibly, which is the reason that we can roughly estimate the instrument sensitivity even without a direct calibration (Ehn et al., 2014). Nevertheless, the large uncertainty must always be kept in mind when interpreting the data.

For HOM formation during Δ^3-carene ozonolysis, the production rate of HOM can be written as $k_1\gamma[carene][O_3]$, where k_1 is carene-O_3 reaction rate coefficient, γ is HOM molar yield, [carene] is Δ^3-carene concentration, and $[O_3]$ is ozone concentration. The losses of HOM arise from condensation on the chamber walls and particles, and flush-out from the chamber (in the case of a continuous-mode chamber). The total loss rate of HOM can be represented as $k_{loss}[HOM]$, where k_{loss} is the total loss rate of HOM.

The COALA chamber was operated in continuous mode, meaning that the inflow of all gases and VOCs was constant. When the chamber reached a steady state, the concentrations of all reactants and products should be constant as well. Therefore, the Equation 1 can be written as:

$$\frac{d[HOM]}{dt} = k_1\gamma[carene][O_3] - k_{loss}[HOM] = 0 \quad (3)$$

$$\Rightarrow \gamma = \frac{k_{loss}[HOM]}{k_1[carene][O_3]} \quad (4)$$

Since no seed particles were injected in the COALA chamber, and the dataset suggested none or only a negligible amount of particles were formed, the total loss rate of HOM was mainly driven by loss to the walls and flush-out. The k_{loss} was determined to be ~ 0.0025 s^{-1} in the COALA chamber. This determination was achieved by modelling the decay of HOM using a simple box model after the removal of O_3 and Δ^3-carene injection at the end of experiment 11. The k_1 was reported to be $3.7\times10^{-17} cm^3 s^{-1}$ at room temperature by Chen et al. (2015).

The AURA chamber was operated in batch mode, meaning that the concentrations of products depended on the cumulative sources and sinks within the chamber. The temporal change in HOM concentrations was not zero, therefore Equation 1 can be written as:

$$\gamma = \frac{k_{loss}[HOM] + \frac{d[HOM]}{dt}}{k_1[carene][O_3]} \quad (5)$$

We observed particle formation for all experiments in the AURA chamber, and thus the loss of HOM (k_{loss}) also included the condensation on particles (CS) in addition to the chamber walls (k_{wall}). We used the method reported by Tuovinen et al. (2021) to estimate CS for HOM monomers and dimers separately for each experiment, and the loss rate to the chamber wall k_{wall} is constant across one experiment and assumed to less than the order of 10^{-3} s^{-1} (Quéléver et al., 2019). The time series of typical CS for HOM monomers and dimers and wall loss across one experiment were shown in Figure S4. Since the temperature-dependent reaction rate of Δ^3-carene ozonolysis has not yet been experimentally determined, in this study, we assumed that the temperature dependence of k_1 is the same as that for α-pinene in MCM: $3.7\times10^{-16}\exp\left(-\frac{640}{T}\right)$ $cm^3\,s^{-1}$, where T represents the chamber temperature. The estimated k_1 at 300 K aligns with the measured value reported by Hantschke et al. (2021). With Equation 5, the molar yield of HOM can be derived as the slope of a linear fit when we plot $k_1[carene][O_3]$ on the x axis and $k_{loss}[HOM] + \frac{d[HOM]}{dt}$ on the y axis.

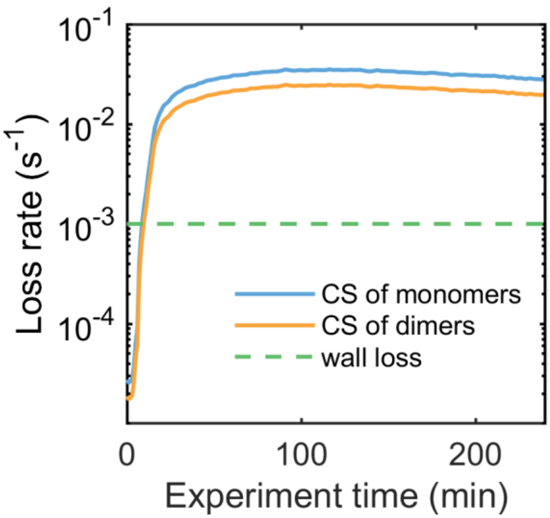

Figure S4. Estimated condensation sink from particles and wall loss rate for HOM in 20B experiment in the AURA chamber.

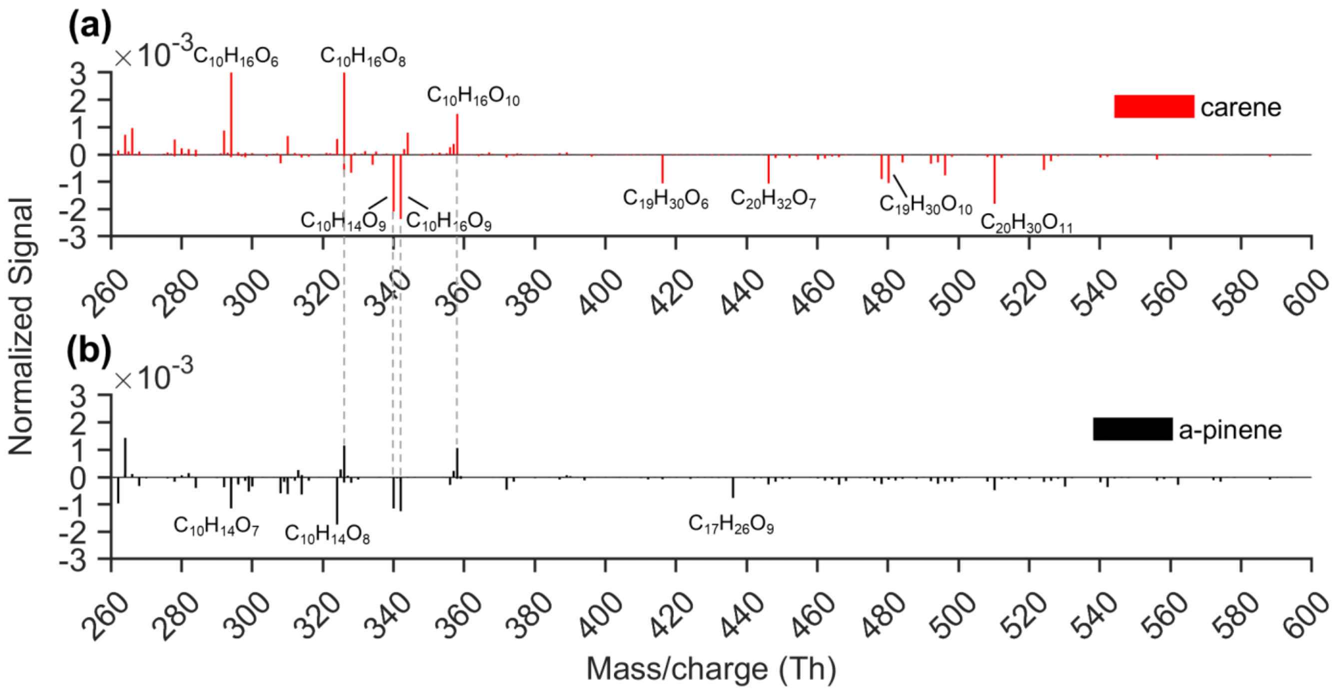

Figure S5. Differential spectrum (diff-spectrum) of carene ozonolysis (a) and α-pinene ozonolysis (b) after CO injection (diff-spectrum = spectrum with CO presence – spectrum before CO injection). The HR (high resolution) the mass spectra from carene and α-pinene ozonolysis were colected under the same conditions (VOC = 20 ppb, O_3 = 30 ppb). All peaks labelled here were detected as a cluster with NO_3^-. Gray dashed lines mark some of the products with the same formulas detected both in carene and α-pinene ozonolysis experiments.

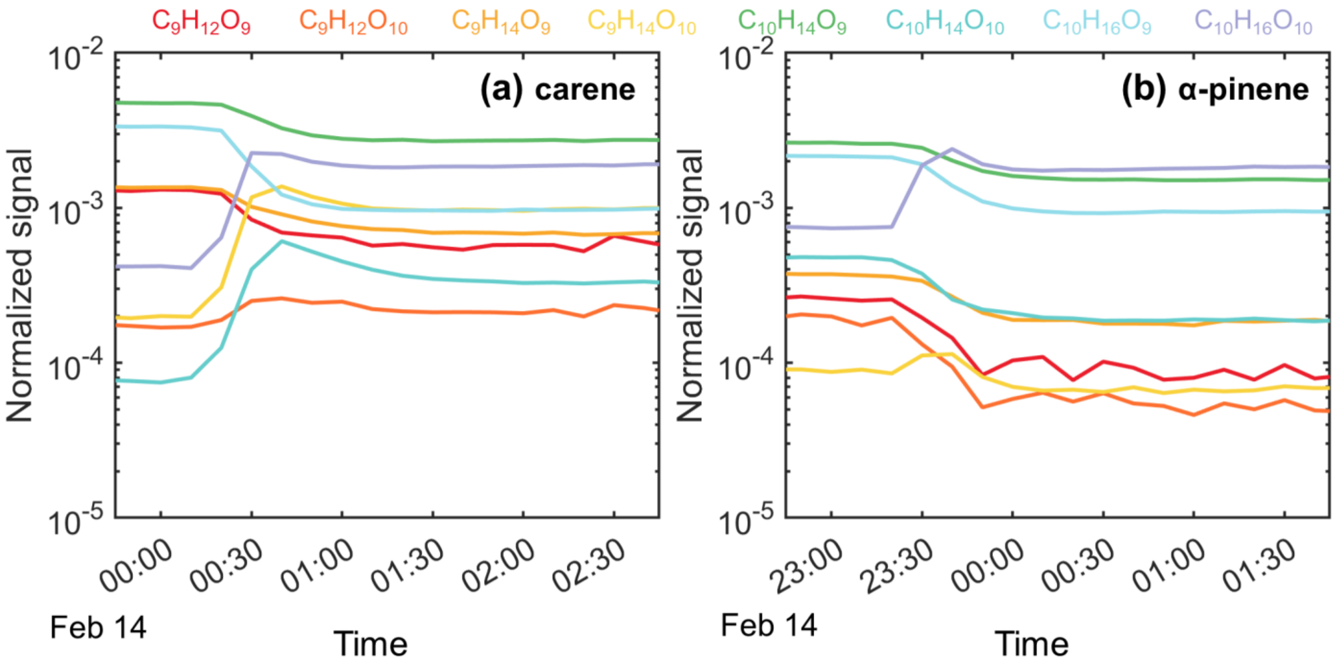

180 **Figure S6. Time series of the selected HOM after injecting CO into carene ozonolysis system (a) and α-pinene ozonolysis system (b) in the COALA chamber.**

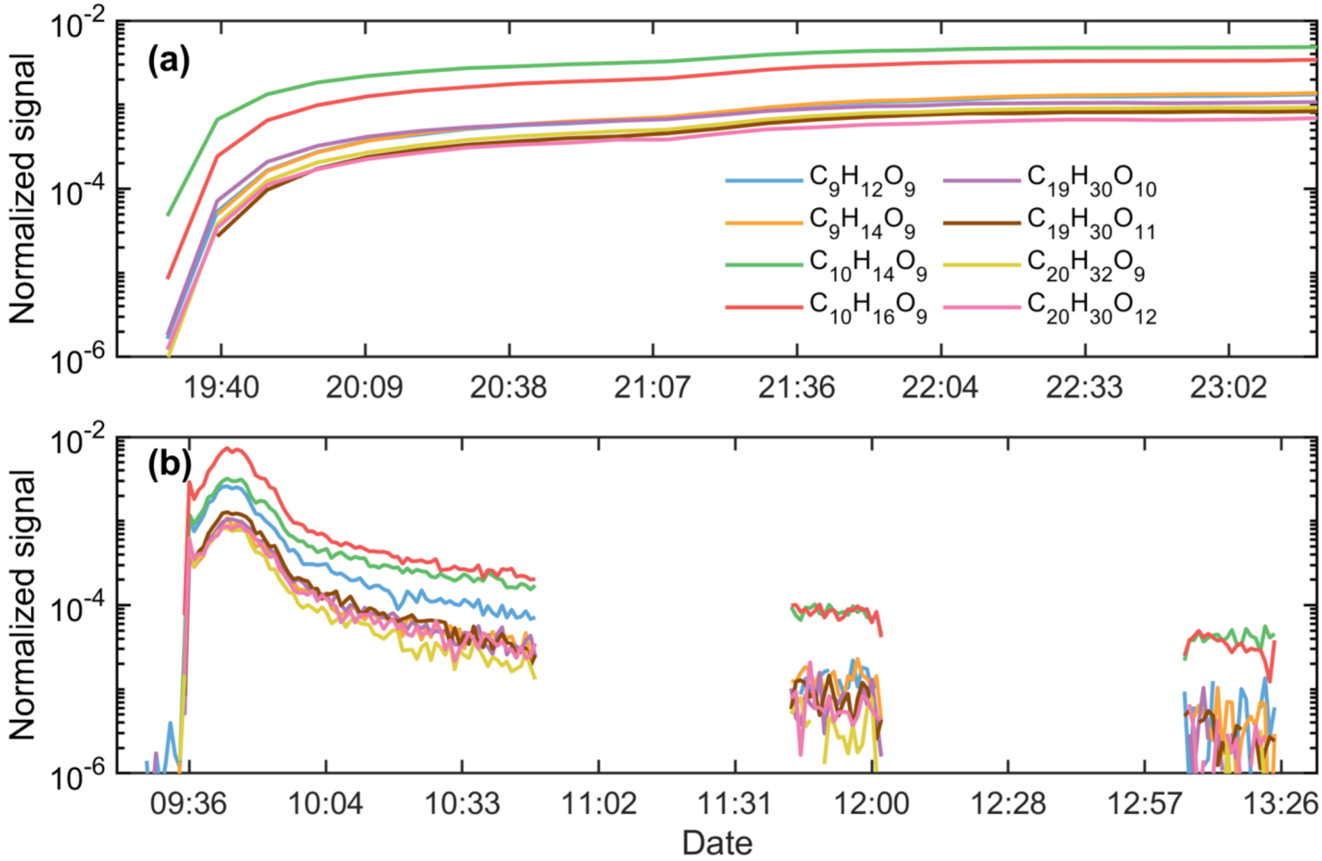

Figure S7. Time series of the selected HOM in the COALA chamber (Experiment 10, panel (a)) and in the AURA chamber (20B, panel (b)).

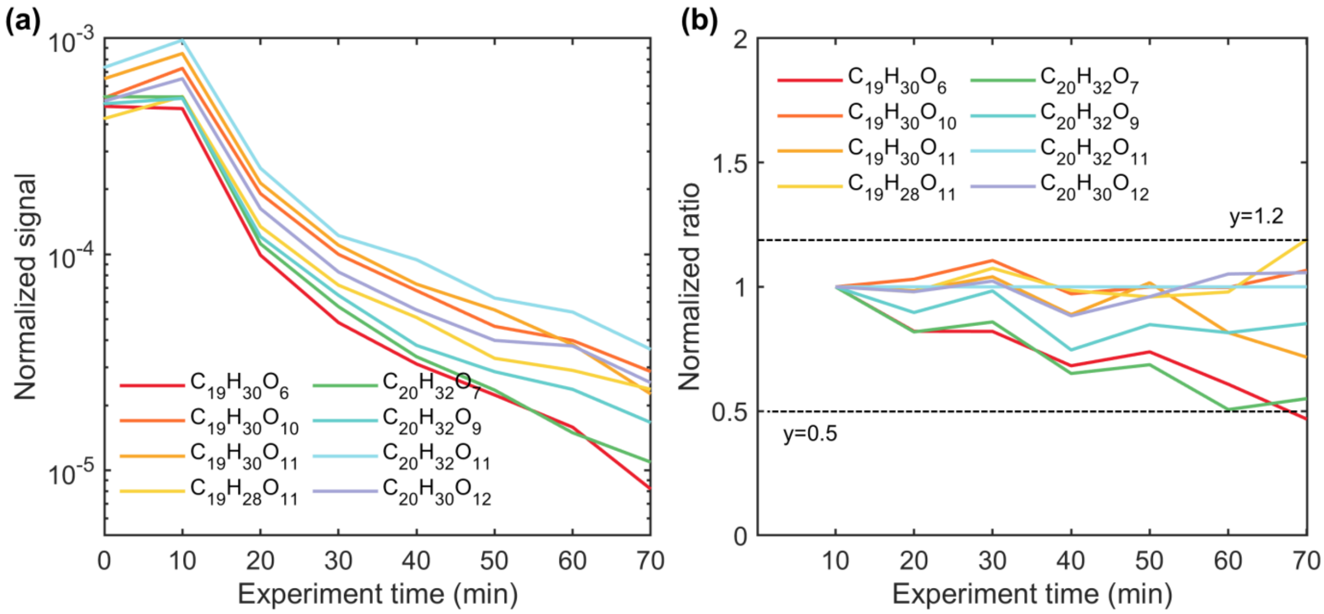

Figure S8. Normalized signal intensity of the largest 8 HOM dimers and the temporal behaviours of the ratios of these dimers (M) to the reference dimer ($C_{20}H_{32}O_{11}$) during the 20B experiment in the AURA chamber. The "normalized ratio" on the y-axis was determined by first calculating the ratio M:$C_{20}H_{32}O_{11}$ at each time point, and this ratio was then normalized by dividing by the ratio value at experiment time=10 min.

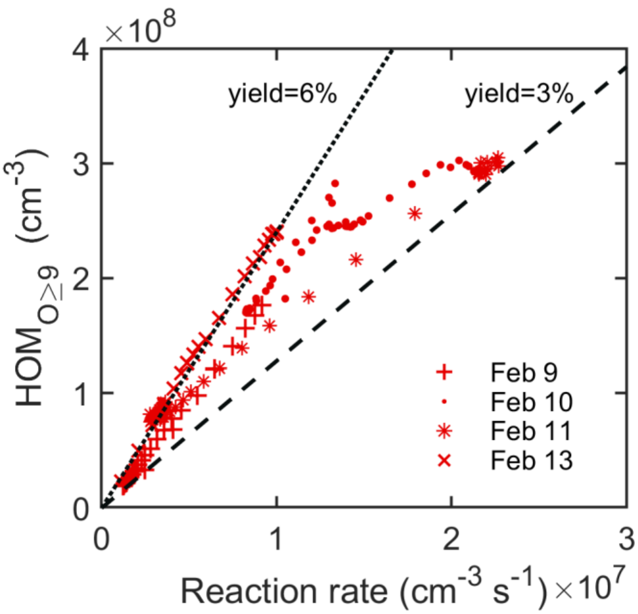

Figure S9. Molar yield of $HOM_{O\geq 9}$ (the sum of HOM monomers with no less than 9 O-atoms and all HOM dimers (O-atoms ≥ 6)) from Δ^3-carene ozonolysis in the COALA chamber at room temperature. Dotted and dashed lines represent the upper and lower limits of the estimated $HOM_{O\geq 9}$ yields.

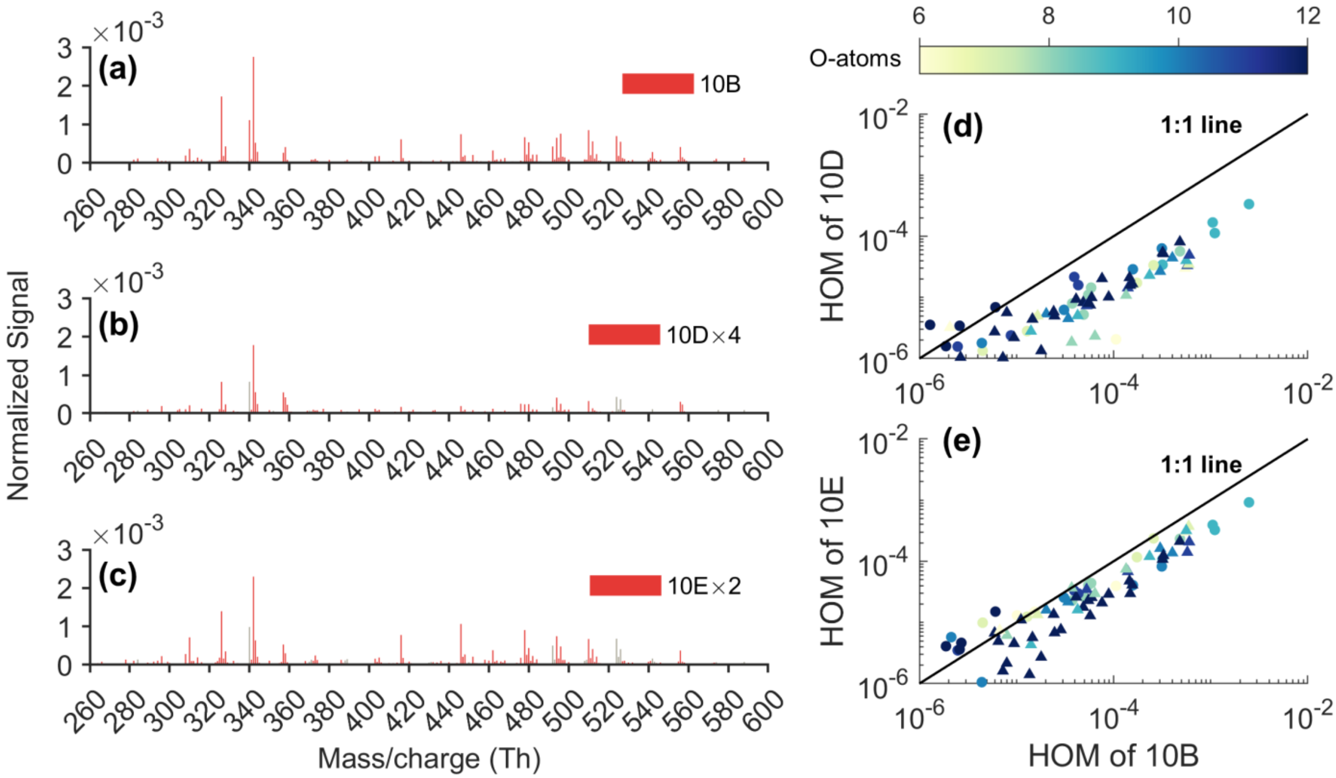

Figure S10. Panels (a)-(c): UMR (unit-mass resolution) mass spectra from 10B (RH < 15%), 10D, and 10 E (RH =80%) carene ozonolysis experiments in the AURA chamber. The grey bars are the water clusters. Panels (d)-(e): Scatter plot of the normalized HOM signal intensity from dry condition experiment (10B) and two high humid experiments (10D and 10E). The signal intensities were multiplied by 4 and 2 in panel (b) and (c), respectively. The circles represent HOM monomers, and the triangles represent HOM dimers. The colour indicates the O-atom content in the identified species.

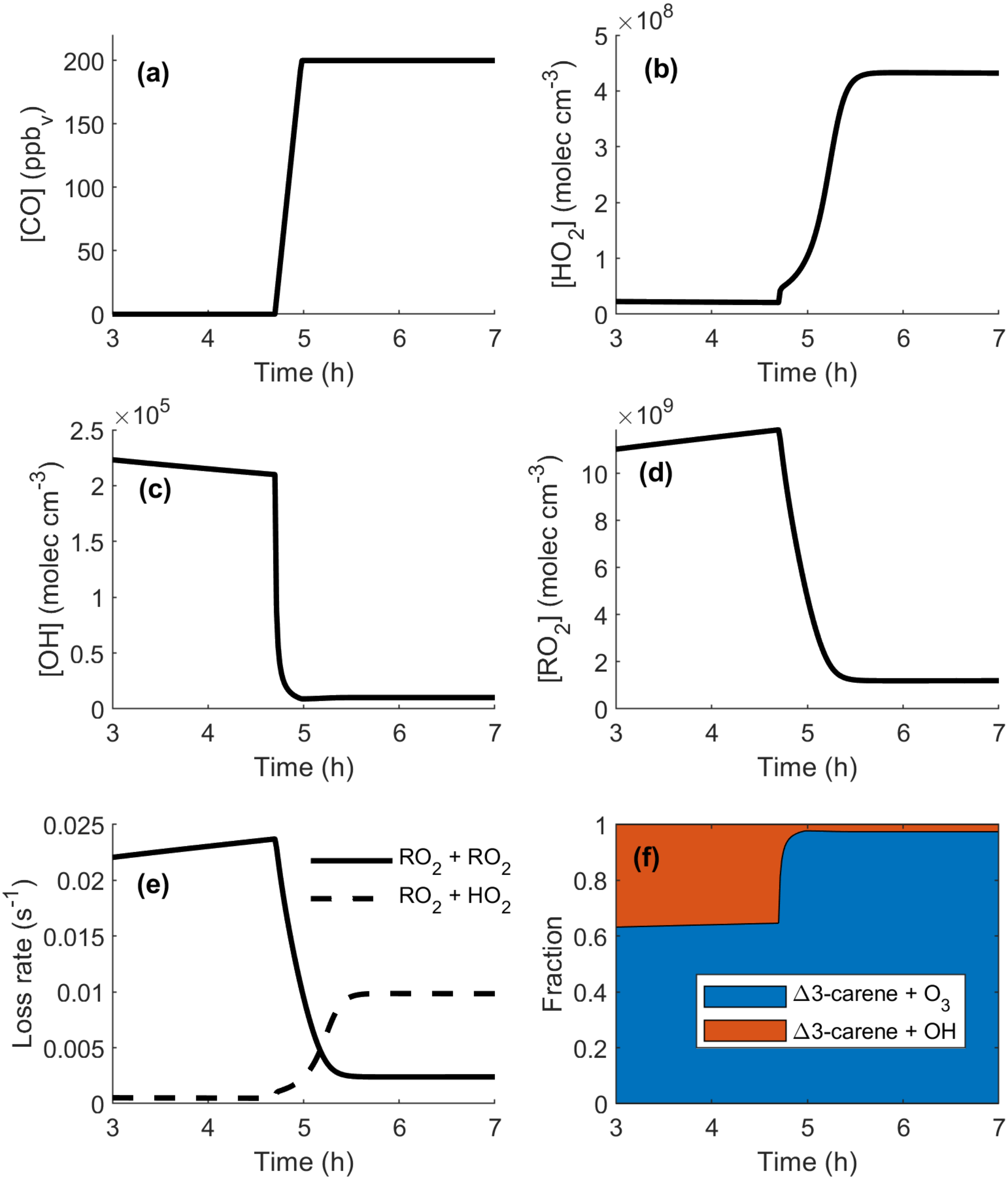

Figure S11. Modelled CO, HO_2, OH and total RO_2 concentrations during the COALA Δ^3-carene ozonolysis experiment with CO addition after ~5 hours (Experiment 10 & 11). Panel (e) shows the modelled loss rate of PRAM RO_2 species because of reactions with RO_2 and HO_2 respectively. Panel (f) shows the modelled fraction of Δ^3-carene that react with ozone and OH respectively.

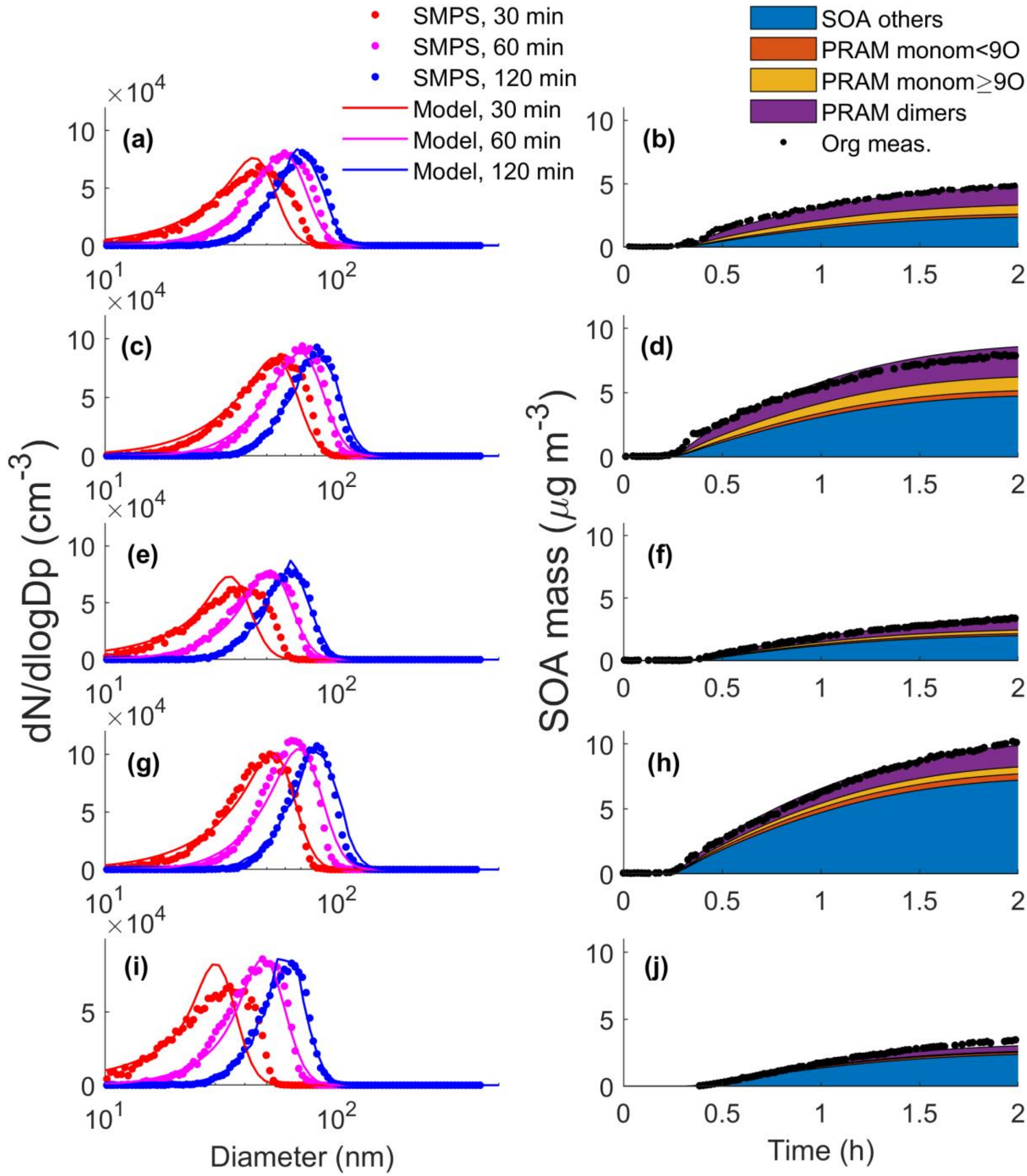

210 **Figure S12. Modelled and measured particle number size distributions and SOA mass concentrations for five different AURA experiments. Panels (a) – (b) show results from exp. 20A (T=20 °C, estimated initial [Δ^3-carene]=9 ppb), panels (c) – (d) results from exp. 20B (T=20 °C, estimated initial [Δ^3-carene]=13.5 ppb), panels (e) – (f) results from exp. 10A (T=10 °C, estimated initial [Δ^3-**

carene]=6.5 ppb), panels (g) – (h) results from exp. 10B (T=10 °C, estimated initial [Δ^3-carene]=13.5 ppb) and panels (i) – (j) results from exp. 0A (T=0 °C, estimated initial [Δ^3-carene]=5.5 ppb).

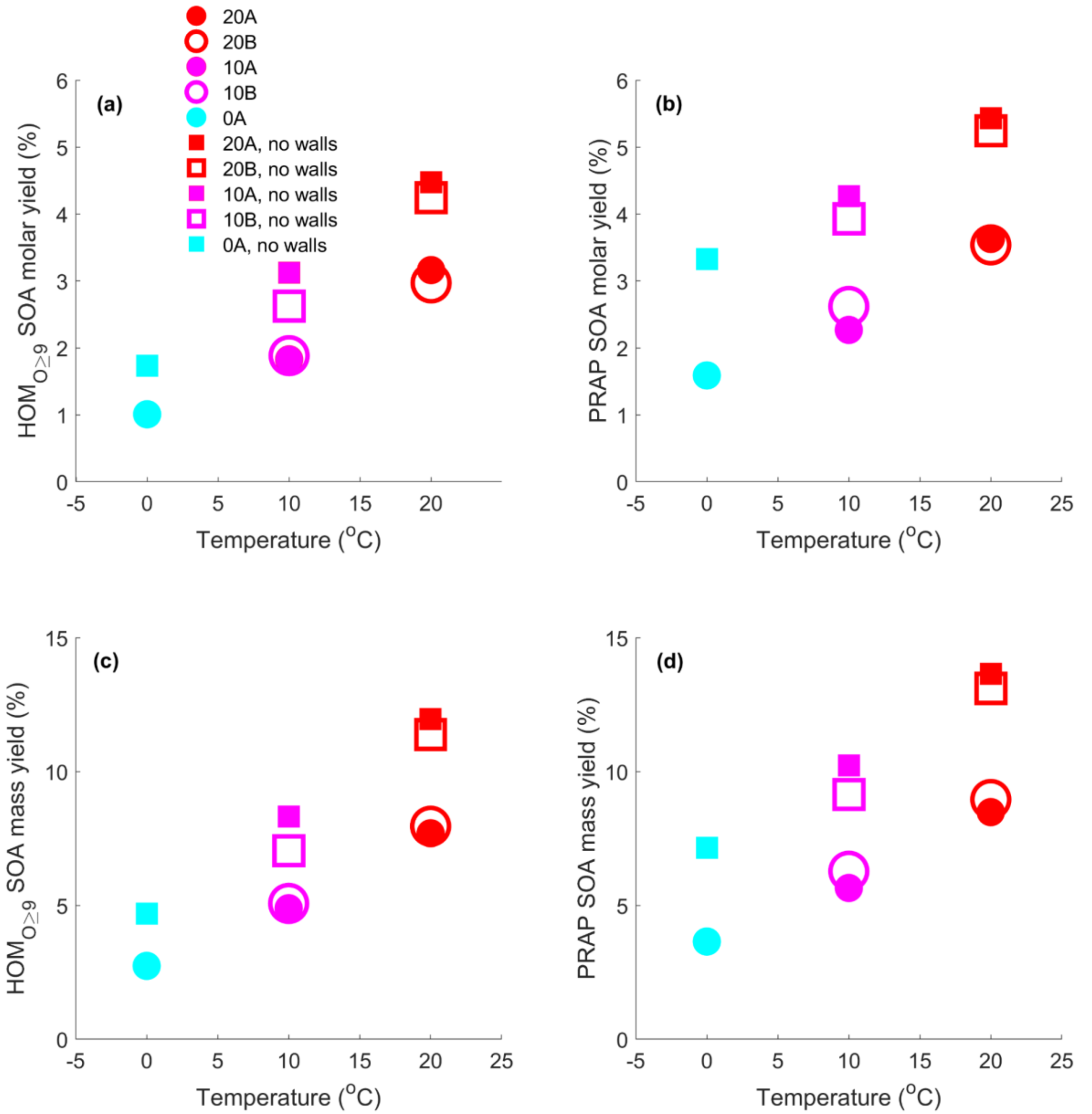

Figure S13. Modelled Peroxy Radical Autoxidation Products (PRAP) SOA yields. Panel (a) and (b) shows modelled molar yields and panel (c) and (d) mass yields. The results are shown both for simulations considering the particle and vapour wall losses in AURA as well as simulations without wall losses (ideal chamber). Panel (a) and (c) shows the HOM$_{O\geq9}$ SOA yields and panel (b) and (d) the total PRAP SOA yields, i.e. all products formed from RO_2 autoxidation that contributed to the SOA mass.

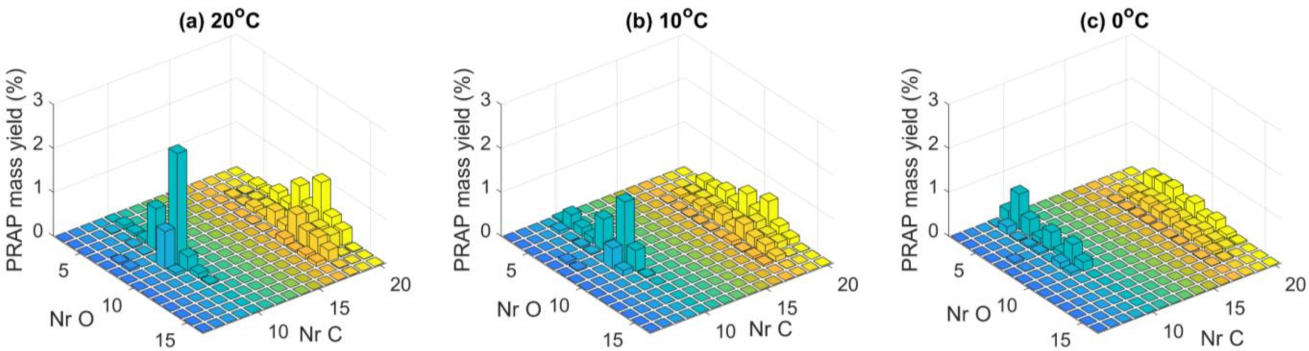

Figure S14. Modelled Peroxy Radical Autoxidation Products (PRAP) SOA yield distribution on a 2-dimensional molecular oxygen and carbon atoms domain for AURA experiment 20A (a), 10A (b) and 0A (c). The monomer distribution (number of C≤10) and dimers (number of C≥17) can be clearly distinguished. The number of oxygen numbers in the PRAP species distribution decreases when the temperature is lowered. This is both a result of slower autoxidation rates and lower saturation vapour pressures at low temperatures.

Tabel S3. Molar yield of initial peroxy radical (RO_2) products that can undergo autoxidation.

Name	Total molar yield after Δ^3-carene + O_3
D3CO2_O4i1	2.75%
D3CO2_O4i2	0.605%
D3CO2_O4i3	1.925%
D3CO2_C9_O4	Maximum ~1.2% if all D3C109O2 react with NO or RO_2

Table S4. Δ^3-carene ozone oxidation chemistry based on proposed initial oxidation steps by Wang et al. (2019), with slight modifications to achieve a 65 % OH yield from the ozonolysis from the initial ozonolysis reaction of Δ^3-carene in accordance with Hantschke et al. (2021). The subsequent multigeneration oxidation mechanism is adopted from the α-pinene mechanism in MCMv3.3.1.

Reactions	Rate constants (cm^3s^{-1})	Notes
D3CARENE + O3 → D3COOA	3.7E-16*EXP(-640/TEMP)*0.5	Criegee intermediate conformer Z-Cl1 in Wang et al. (2019)
D3CARENE + O3 → D3COOB	3.7E-16*EXP(-640/TEMP)*0.2	Criegee intermediate conformer Z-Cl2 in Wang et al. (2019)
D3CARENE + O3 → D3COOC	3.7E-16*EXP(-640/TEMP)*0.3	Criegee intermediate conformer E-Cl1 in Wang et al. (2019)
D3COOA → D3CSOZ	0.5*KDEC	Secondary ozonoide (SOZ) formation based on Wang et al. (2019)
D3COOA → D3CVHP1	0.5*KDEC	Vinyl hydroperoxide (VHP) product 1, VHP1 in Wang et al. (2019), Schemes 1 and 4

D3COOB → D3CSOZ	0.5*KDEC	Secondary ozonoide (SOZ) formation based on Wang et al. (2019)
D3COOB → D3CVHP2	0.5*KDEC	Vinyl hydroperoxide (VHP) product 2, VHP2 in Wang et al. (2019), Scheme 1
D3COOC → D3CVHP1	KDEC	Vinyl hydroperoxide (VHP) product 1, VHP1 in Wang et al. (2019), Schemes 1 and 4
D3CSOZ → D3CONIC	KDEC	cis-3-caronic acid formation, 35 % production yield
D3CONIC + OH → D3C96O2 + CO + OH	6.65E-12	
D3CVHP1 → D3C109O2 + OH	KDEC*0.904	D3C109O2 analogous to MCMv3.3.1 α-pinene ozonolysis product C109O2
D3CVHP1 → D3CO2_O4i1 + OH	KDEC*0.05	Reaction leading to C_{10} RO_2 autoxidation products
D3CVHP1 → D3CO2_O4i2 + OH	KDEC*0.011	Reaction leading to C_{10} RO_2 autoxidation products
D3CVHP1 → D3CO2_O4i3 + OH	KDEC*0.035	Reaction leading to C_{10} RO_2 autoxidation products
D3CVHP2 → D3C107O2 + OH	KDEC	
Continued multigeneration oxidation chemistry analogous to MCMv3.3.1 a-pinene C109O2 product reaction pathway		
D3C109O2 + HO2 → D3C109OOH	KRO2HO2*0.914	
D3C109O2 + NO → D3C109O + NO2	KRO2NO	
D3C109O2 + NO3 → D3C109O + NO2	KRO2NO3	
D3C109O2 → D3C109CO	1.00E-11*RO2*0.05	
D3C109O2 → D3C109O	1.00E-11*RO2*0.95	
D3C109O2 → D3C109OH	1.00E-11*RO2*0.05*0.0	
D3C109O → D3C89CO3 + HCHO	KDEC*0.88	
D3C109O → D3C920CO3	KDEC*0.1	
D3C109O → D3CO2_C9_O4 + HCHO	KDEC*0.02	Reaction leading to C_9 RO_2 autoxidation products
D3C109OOH + OH → D3C109CO + OH	5.47E-11	
D3C109OOH → D3C109O + OH	J(41)+J(15)	Photolysis reaction
D3C109OOH → D3C89CO3 + HCHO + OH	J(22)	Photolysis reaction
D3C109CO + OH → D3C89CO3 + CO	5.47E-11	
D3C109CO → D3C89CO3 + CO + HO2	J(34)+J(15)	Photolysis reaction
D3C109OH + OH → D3C109CO + HO2	4.45E-11	
D3C109OH → D3C89CO3 + HCHO + HO2	J(22)	Photolysis reaction
D3C109OH → D3C920O2 + CO + HO2	J(15)	Photolysis reaction
D3C89CO3 + HO2 → D3C89CO2 + OH	KAPHO2*0.44	
D3C89CO3 + HO2 → D3C89CO2H + O3	KAPHO2*0.15	
D3C89CO3 + HO2 → D3C89CO3H	KAPHO2*0.41	
D3C89CO3 + NO → D3C89CO2 + NO2	KAPNO	
D3C89CO3 + NO2 → D3C89PAN	KFPAN	

D3C89CO3 + NO3 → D3C89CO2 + NO2	KRO2NO3*1.74	
D3C89CO3 → D3C89CO2	1.00E-11*RO2*0.7	
D3C89CO3 → D3C89CO2H	1.00E-11*RO2*0.3	
D3C89CO2 → D3C811CO3	KDEC*0.8000	
D3C89CO2 → D3C89O2	KDEC*0.2000	
D3C89CO2H + OH → D3C89CO2	2.69E-11	
D3C89CO2H → D3C89CO2 + HO2	J(15)	Photolysis reaction
D3C89CO3H + OH → D3C89CO3	3.00E-11	
D3C89CO3H → D3C89CO2 + OH	J(41)+J(15)	Photolysis reaction
D3C89PAN + OH → CH3COCH3 + CO13C4CHO + CO + NO2	2.52E-11	
D3C89PAN → D3C89CO3 + NO2	KBPAN	
D3C89O2 + HO2 → D3C89OOH	KRO2HO2*0.859	
D3C89O2 + NO → D3C89NO3	KRO2NO*0.104	
D3C89O2 + NO → D3C89O + NO2	KRO2NO*0.896	
D3C89O2 + NO3 → D3C89O + NO2	KRO2NO3	
D3C89O2 → D3C89O	6.70E-15*RO2*0.7	
D3C89O2 → D3C89OH	6.70E-15*RO2*0.3	
D3C89OOH + OH → D3C89O2	3.61E-11	
D3C89OOH → D3C89O + OH	J(41)+J(15)	Photolysis reaction
D3C89NO3 + OH → CH3COCH3 + CO13C4CHO + NO2	2.56E-11	
D3C89NO3 → D3C89O + NO2	J(55)+J(15)	Photolysis reaction
D3C89O → D3C810O2	2.70D+14*EXP(-6643/TEMP)	
D3C89OH + OH → D3C89O	2.86E-11	
D3C89OH → D3C89O + HO2	J(15)	Photolysis reaction
D3C920CO3 + HO2 → D3C920CO3H	KAPHO2*0.41	
D3C920CO3 + HO2 → D3C920O2 + OH	KAPHO2*0.44	
D3C920CO3 + HO2 → HOD3CONIC + O3	KAPHO2*0.15	OH-3-caronic acid formation
D3C920CO3 + NO → D3C920O2 + NO2	KAPNO	
D3C920CO3 + NO2 → D3C920PAN	KFPAN	
D3C920CO3 + NO3 → D3C920O2 + NO2	KRO2NO3*1.74	
D3C920CO3 → D3C920O2	1.00E-11*RO2*0.70	
D3C920CO3 → HOD3CONIC	1.00E-11*RO2*0.30	OH-3-caronic acid formation
D3C920O2 + HO2 → D3C920OOH	KRO2HO2*0.890	
D3C920O2 + NO → D3C920O + NO2	KRO2NO	
D3C920O2 + NO3 → D3C920O + NO2	KRO2NO3	
D3C920O2 → D3C920O	1.30E-12*RO2	
D3C920CO3H + OH → D3C920CO3	9.16E-12	
D3C920CO3H → D3C920O2 + OH	J(41)+J(22)	Photolysis reaction
D3C920PAN + OH → D3C109OH + CO + NO2	5.56E-12	

D3C920PAN → D3C920CO3 + NO2	KBPAN	
D3C920OOH + OH → D3C920O2	2.36E-11	
D3C920OOH → D3C920O + OH	J(41)+J(22)	Photolysis reaction
D3C920O → D3C921O2	4.20D+10*EXP(-3523/TEMP)	
D3C811CO3 + HO2 → D3C811CO3H	KAPHO2*0.4100	
D3C811CO3 + HO2 → D3C811O2 + OH	KAPHO2*0.4400	
D3C811CO3 + HO2 → D3CIC + O3	KAPHO2*0.1500	cis-3-caric acid formation
D3C811CO3 + NO → D3C811O2 + NO2	KAPNO	
D3C811CO3 + NO2 → D3C811PAN	KFPAN	
D3C811CO3 + NO3 → D3C811O2 + NO2	KRO2NO3*1.74	
D3C811CO3 → D3C811O2	1.0001E-11*RO2*0.70	
D3C811CO3 → D3CIC	1.0001E-11*RO2*0.30	cis-3-caric acid formation
D3C811CO3H + OH → D3C811CO3	1.04E-11	
D3C811CO3H → D3C811O2 + OH	J(41)	Photolysis reaction
D3C811O2 + HO2 → D3C811OOH	KRO2HO2*0.859	
D3C811O2 + NO → D3C811NO3	KRO2NO*0.138	
D3C811O2 + NO → D3C811O + NO2	KRO2NO*0.862	
D3C811O2 + NO3 → D3C811O + NO2	KRO2NO3	
D3C811O2 → D3C721CHO	1.30E-12*RO2*0.2	
D3C811O2 → D3C811O	1.30E-12*RO2*0.6	
D3C811O2 → D3C811OH	1.30E-12*RO2*0.2	
D3CIC + OH → D3C811O2	7.29E-12	
D3C811PAN + OH → D3C721CHO + CO + NO2	6.77E-12	
D3C811PAN → D3C811CO3 + NO2	KBPAN	
D3C811OOH + OH → D3C721CHO + OH	1.70E-11	
D3C811OOH → D3C811O + OH	J(41)	Photolysis reaction
D3C811NO3 + OH → D3C721CHO + NO2	3.29E-12	
D3C811NO3 → D3C811O + NO2	J(53)	Photolysis reaction
D3C811O → D3C812O2	KDEC	
D3C811OH + OH → D3C721CHO + HO2	7.89E-12	
D3C810O2 + HO2 → D3C810OOH	KRO2HO2*0.914	
D3C810O2 + NO → D3C810NO3	KRO2NO*0.104	
D3C810O2 + NO → D3C810O + NO2	KRO2NO*0.896	
D3C810O2 + NO3 → D3C810O + NO2	KRO2NO3	
D3C810O2 → D3C810O	6.70E-15*RO2*0.7	
D3C810O2 → D3C810OH	6.70E-15*RO2*0.3	
D3C810OOH + OH → D3C810O2	8.35E-11	
D3C810OOH → D3C810O + OH	J(41)+J(15)	Photolysis reaction
D3C810NO3 + OH → CH3COCH3 + CO13C4CHO + NO2	4.96E-11	
D3C810NO3 → D3C810O + NO2	J(55)+J(15)	Photolysis reaction

D3C810O → CH3COCH3 + C514O2	2.70D+14*EXP(-6643/TEMP)	
D3C810OH + OH → D3C810O	8.00E-11	
D3C810OH → D3C810O + HO2	J(15)	Photolysis reaction
D3C812O2 + HO2 → D3C812OOH	KRO2HO2*0.859	
D3C812O2 + NO → D3C812O + NO2	KRO2NO	
D3C812O2 + NO3 → D3C812O + NO2	KRO2NO3	
D3C812O2 → D3C812O	9.20E-14*RO2*0.7	
D3C812O2 → D3C812OH	9.20E-14*RO2*0.3	
D3C812OOH + OH → D3C812O2	1.09E-11	
D3C812OOH → D3C812O + OH	J(41)	Photolysis reaction
D3C812O → D3C813O2	KDEC	
D3C812OH + OH → D3C812O	7.42E-12	
D3C813O2 + HO2 → D3C813OOH	KRO2HO2*0.859	
D3C813O2 + NO → D3C813NO3	KRO2NO*0.104	
D3C813O2 + NO → D3C813O + NO2	KRO2NO*0.896	
D3C813O2 + NO3 → D3C813O + NO2	KRO2NO3	
D3C813O2 → D3C813O	6.70E-15*RO2*0.7	
D3C813O2 → D3C813OH	6.70E-15*RO2*0.3	
D3C813OOH + OH → D3C813O2	1.86E-11	
D3C813OOH → D3C813O + OH	J(41)+J(34)	Photolysis reaction
D3C813NO3 + OH → CH3COCH3 + CO13C3CO2H + HCHO + NO2	7.82E-12	
D3C813NO3 → D3C813O + NO2	J(55)+J(34)	Photolysis reaction
D3C813O → CH3COCH3 + C516O2	KDEC	
D3C813OH + OH → D3C813O	1.75E-11	
D3C813OH → D3C813O + HO2	J(34)	Photolysis reaction
D3C921O2 + HO2 → D3C921OOH	KRO2HO2*0.890	
D3C921O2 + NO → D3C921O + NO2	KRO2NO	
D3C921O2 + NO3 → D3C921O + NO2	KRO2NO3	
D3C921O2 → D3C921O	6.70E-15*RO2	
D3C921OOH + OH → D3C921O2	1.29E-11	
D3C921OOH → D3C921O + OH	J(41)+J(22)	Photolysis reaction
D3C921O → D3C922O2	KDEC	
D3C922O2 + HO2 → D3C922OOH	KRO2HO2*0.890	
D3C922O2 + NO → D3C922O + NO2	KRO2NO	
D3C922O2 + NO3 → D3C922O + NO2	KRO2NO3	
D3C922O2 → D3C922O	6.70E-15*RO2	
D3C922OOH + OH → D3C922O2	1.51E-11	
D3C922OOH → D3C922O + OH	J(41)+J(22)	Photolysis reaction
D3C922O → CH3COCH3 + C621O2	KDEC	

D3C96O2 + HO2 → D3C96OOH	KRO2HO2*0.890	
D3C96O2 + NO → D3C96NO3	KRO2NO*0.157	
D3C96O2 + NO → D3C96O + NO2	KRO2NO*0.843	
D3C96O2 + NO3 → D3C96O + NO2	KRO2NO3	
D3C96O2 → D3C96O	1.30E-12*0.6*RO2	
D3C96O2 → D3C96OH	1.30E-12*0.2*RO2	
D3C96O2 → NORD3CAL	1.30E-12*0.2*RO2	
D3C96CO3 + HO2 → D3C96O2 + OH	KAPHO2*0.44	
D3C96CO3 + HO2 → PERD3CONIC	KAPHO2*0.41	
D3C96CO3 + HO2 → D3CONIC + O3	KAPHO2*0.15	cis-3-caronic acid formation
D3C96CO3 + NO → D3C96O2 + NO2	KAPNO	
D3C96CO3 + NO2 → D3CPAN	KFPAN	
D3C96CO3 + NO3 → D3C96O2 + NO2	KRO2NO3*1.74	
D3C96CO3 → D3C96O2	1.00E-11*0.7*RO2	
D3C96CO3 → D3CONIC	1.00E-11*0.3*RO2	cis-3-caronic acid formation
D3C96OOH + OH → D3C96O2	1.90E-12*EXP(190/TEMP)	
D3C96OOH + OH → NORD3CAL + OH	1.30E-11	
D3C96OOH → D3C96O + OH	J(41)+J(22)	Photolysis reaction
D3C96NO3 + OH → NORD3CAL + NO2	2.88E-12	
D3C96NO3 → D3C96O + NO2	J(53)+J(22)	Photolysis reaction
D3C96O → D3C97O2	4.20D+10*EXP(-3523/TEMP)	
D3C96OH + OH → NORD3CAL + HO2	7.67E-12	
D3C96OH → D3C96O + HO2	J(22)	Photolysis reaction
D3CPAN + OH → NORD3CAL + CO + NO2	3.66E-12	
D3CPAN → D3C96CO3 + NO2	KBPAN	
PERCANONIC + OH → D3C96CO3	9.73E-12	
PERCANONIC → D3C96O2 + OH	J(41)+J(22)	Photolysis reaction
NORD3CAL + NO3 → D3C85CO3 + HNO3	KNO3AL*8.5	
NORD3CAL + OH → D3C85CO3	2.64E-11	
NORD3CAL → D3C85O2 + CO + HO2	J(15)	Photolysis reaction
D3C85CO3 + HO2 → D3C85CO3H	KAPHO2*0.56	
D3C85CO3 + HO2 → D3C85O2 + OH	KAPHO2*0.44	
D3C85CO3 + NO → D3C85O2 + NO2	KAPNO	
D3C85CO3 + NO2 → D3C9PAN	KFPAN	
D3C85CO3 + NO3 → D3C85O2 + NO2	KRO2NO3*1.74	
D3C85CO3 → D3C85O2	1.00E-11*RO2	
D3C85O2 + HO2 → D3C85OOH	KRO2HO2*0.859	
D3C85O2 + NO → D3C85O + NO2	KRO2NO	
D3C85O2 + NO3 → D3C85O + NO2	KRO2NO3	
D3C85O2 → D3C85O	6.70E-15*RO2	

D3C85CO3H + OH → D3C85CO3	1.02E-11	
D3C85CO3H → D3C85O2 + OH	J(41)+J(22)	Photolysis reaction
D3C9PAN + OH → D3C85OOH + CO + NO2	6.60E-12	
D3C9PAN → D3C85CO3 + NO2	KBPAN	
D3C85OOH + OH → D3C85O2	1.29E-11	
D3C85OOH → D3C85O + OH	J(41)+J(22)	Photolysis reaction
D3C85O → D3C86O2	KDEC	
D3C86O2 + HO2 → D3C86OOH	KRO2HO2*0.859	
D3C86O2 + NO → D3C86O + NO2	KRO2NO	
D3C86O2 + NO3 → D3C86O + NO2	KRO2NO3	
D3C86O2 → D3C86O	6.70E-15*RO2	
D3C86OOH + OH → D3C86O2	3.45E-11	
D3C86OOH → D3C86O + OH	J(41)+J(15)	Photolysis reaction
D3C86O → C511O2 + CH3COCH3	KDEC	
Chemistry based on MCM APINENE chemistry C107O2		
D3C107O2 + HO2 → D3C107OOH	KRO2HO2*0.914	
D3C107O2 + NO → D3C107O + NO2	KRO2NO	
D3C107O2 + NO3 → D3C107O + NO2	KRO2NO3	
D3C107O2 → D3C107O	9.20E-14*0.7*RO2	
D3C107O2 → D3C107OH	9.20E-14*0.3*RO2	
D3C107OOH + OH → D3C107O2	3.01E-11	
D3C107OOH → D3C107O + OH	J(41)+J(15)	Photolysis reaction
D3C107O → D3C108O2	KDEC	
D3C107OH + OH → D3C107O	2.66E-11	
D3C107OH → D3C107O + HO2	J(15)	Photolysis reaction
D3C108O2 + HO2 → D3C108OOH	KRO2HO2*0.914	
D3C108O2 + NO → D3C108NO3	KRO2NO*0.125	
D3C108O2 + NO → D3C108O + NO2	KRO2NO*0.875	
D3C108O2 + NO3 → D3C108O + NO2	KRO2NO3	
D3C108O2 → D3C108O	6.70E-15*0.7*RO2	
D3C108O2 → D3C108OH	6.70E-15*0.3*RO2	
D3C108OOH + OH → D3C108O2	6.28E-11	
D3C108OOH → D3C108O + OH	J(41)+J(35)	Photolysis reaction
D3C108NO3 + OH → CO235C6CHO + CH3COCH3 + NO2	2.85E-11	
D3C108NO3 → D3C108O + NO2	J(55)+J(35)	Photolysis reaction
D3C108O → C717O2 + CH3COCH3	KDEC	
D3C108OH + OH → D3C108O	5.93E-11	
D3C108OH → D3C108O + HO2	J(35)	Photolysis reaction
D3C97O2 + HO2 → D3C97OOH	KRO2HO2*0.890	
D3C97O2 + NO → D3C97O + NO2	KRO2NO	

D3C97O2 + NO3 → D3C97O + NO2	KRO2NO3	
D3C97O2 → D3C97O	6.70E-15*0.7*RO2	
D3C97O2 → D3C97OH	6.70E-15*0.3*RO2	
D3C97OOH + OH → D3C97O2	1.05E-11	
D3C97OOH → D3C97O + OH	J(41)+J(22)	Photolysis reaction
D3C97O → D3C98O2	KDEC	
D3C97OH + OH → D3C97O	7.20E-12	
D3C97OH → D3C97O + HO2	J(22)	Photolysis reaction
D3C98O2 + HO2 → D3C98OOH	KRO2HO2*0.890	
D3C98O2 + NO → D3C98NO3	KRO2NO*0.118	
D3C98O2 + NO → D3C98O + NO2	KRO2NO*0.882	
D3C98O2 + NO3 → D3C98O + NO2	KRO2NO3	
D3C98O2 → D3C98O	6.70E-15*0.7*RO2	
D3C98O2 → D3C98OH	6.70E-15*0.3*RO2	
D3C98OOH + OH → D3C98O2	2.05E-11	
D3C98OOH → D3C98O + OH	J(41)+J(35)	Photolysis reaction
D3C98NO3 + OH → CH3COCH3 + C614CO + NO2	5.37E-12	
D3C98NO3 → D3C98O + NO2	J(55)+J(35)	Photolysis reaction
D3C98O → C614O2 + CH3COCH3	KDEC	
D3C98OH + OH → D3C98O	1.69E-11	
D3C98OH → D3C98O + HO2	J(35)	Photolysis reaction
D3C721CHO + NO3 → D3C721CO3 + HNO3	KNO3AL*8.5	
D3C721CHO + OH → D3C721CO3	2.63E-11	
D3C721CHO → D3C721O2 + CO + HO2	J(15)	Photolysis reaction
D3C721CO3 + HO2 → D3C721CO3H	KAPHO2*0.41	
D3C721CO3 + HO2 → D3C721O2 + OH	KAPHO2*0.44	
D3C721CO3 + HO2 → NORD3CIC + O3	KAPHO2*0.15	
D3C721CO3 + NO → D3C721O2 + NO2	KAPNO	
D3C721CO3 + NO2 → D3C721PAN	KFPAN	
D3C721CO3 + NO3 → D3C721O2 + NO2	KRO2NO3*1.74	
D3C721CO3 → D3C721O2	1.00E-11*RO2*0.7	
D3C721CO3 → NORD3CIC	1.00E-11*RO2*0.3	
D3C721O2 + HO2 → D3C721OOH	KRO2HO2*0.820	
D3C721O2 + NO → D3C721O + NO2	KRO2NO	
D3C721O2 + NO3 → D3C721O + NO2	KRO2NO3	
D3C721O2 → D3C721O	1.30E-12*RO2	
D3C721CO3H + OH → D3C721CO3	9.65E-12	
D3C721CO3H → D3C721O2 + OH	J(41)	Photolysis reaction
D3C721PAN + OH → D3C721OOH + CO + NO2	2.96E-12	
D3C721PAN → D3C721CO3 + NO2	KBPAN	

D3C721OOH + OH → D3C721O2	1.27E-11	
D3C721OOH → D3C721O + OH	J(41)	Photolysis reaction
D3C721O → C722O2	KDEC	
NORD3CIC + OH → D3C721O2	6.57E-12	

235 **Table S5. Δ^3-carene OH oxidation mechanism based on Hantschke et al. (2021) and analogous reactions as for α-pinene in MCMv3.3.1.**

Reactions	Rate constants (cm^3s^{-1})	Notes
D3CENE + OH → D3C1O2	0.6*2.48E-11*EXP(357./TEMP)	Absolute rate from Dillon et al. (2017)
D3CENE + OH → D3C2O2	0.4*2.48E-11*EXP(357./TEMP)	Absolute rate from Dillon et al. (2017)
D3C1O2 + NO → D3CO	0.77*KRO2NO	Analogous to APINBO2 reactions in MCMv3.3.1
D3C1O2 + NO → D3C1NO3	0.23*KRO2NO	Analogous to APINBO2 reactions in MCMv3.3.1
D3C1O2 + HO2 → D3C1OOH	KRO2HO2*0.914	Analogous to APINBO2 reactions in MCMv3.3.1
D3C1O2 + NO3 → D3CO	KRO2NO3	Analogous to APINBO2 reactions in MCMv3.3.1
D3C1O2 → D3CO	0.6*RO2*8.8E-13	Analogous to APINBO2 reactions in MCMv3.3.1
D3C1O2 → D3COH	0.2*RO2*8.8E-13	Analogous to APINBO2 reactions in MCMv3.3.1
D3C1O2 → D3CCO	0.2*RO2*8.8E-13	Analogous to APINBO2 reactions in MCMv3.3.1
D3C2O2 + NO → D3CO	0.77*KRO2NO	Analogous to APINAO2 reactions in MCMv3.3.1
D3C2O2 + NO → D3C2NO3	0.23*KRO2NO	Analogous to APINAO2 reactions in MCMv3.3.1
D3C2O2 + HO2 → D3C2OOH	KRO2HO2*0.914	Analogous to APINAO2 reactions in MCMv3.3.1
D3C2O2 + NO3 → D3CO	KRO2NO3	Analogous to APINAO2 reactions in MCMv3.3.1
D3C2O2 → D3CO	0.7*RO2*9.4E-14	Analogous to APINAO2 reactions in MCMv3.3.1
D3C2O2 → D3COH	0.3*RO2*9.4E-14	Analogous to APINAO2 reactions in MCMv3.3.1
D3CO → D3CAL + HO2	KDEC*0.997	3-caronaldehyde formation
D3CO → D3CO2_OH_O4i3	KDEC*0.003	
D3CAL + OH → D3C96CO3	0.772*4.1E-11	Analogous to PINAL (pinonaldehyde) in MCMv3.3.1
D3CAL + OH → D3CALO2	0.228*4.1E-11	Analogous to PINAL (pinonaldehyde) in MCMv3.3.1
D3CAL → D3C96O2	J(15)	Analogous to PINAL (pinonaldehyde) in MCMv3.3.1
D3COH + OH → D3CCO + HO2	1.49E-11	
D3C2OOH + OH → D3C2O2	1.83E-11	
D3C2OOH → D3CO + OH	J(41)	Photolysis reaction

D3C1OOH + OH → D3CCO + OH	3.28E-11	
D3C1OOH → D3CO + OH	J(41)	Photolysis reaction
D3C1NO3 + OH → D3CCO + NO2	3.64E-12	
D3C2NO3 + OH → D3CAL + NO2	5.5E-12	
D3CCO + OH → D3C96CO3	8.18E-12	
D3CALO2 + HO2 → D3CALOOH	KRO2HO2*0.914	
D3CALO2 + NO → D3CALNO3	KRO2NO*0.050	
D3CALO2 + NO → D3CALO + NO2	KRO2NO*0.950	
D3CALO2 + NO3 → D3CALO + NO2	KRO2NO3	
D3CALO2 → D3CALO	6.70E-15*0.7*RO2	
D3CALO2 → D3CALOH	6.70E-15*0.3*RO2	
D3CALOOH + OH → D3CALO2	2.75E-11	
D3CALOOH → D3CALO + OH	J(41)+J(15)	Photolysis reaction
D3CALNO3 + OH → CO235C6CHO + CH3COCH3 + NO2	2.25E-11	
D3CALNO3 → D3CALO + NO2	J(55)+J(15)	Photolysis reaction
D3CALO → D3C106O2	KDEC	
D3CALOH + OH → D3CALO	2.41E-11	
D3CALOH → D3CALO + HO2	J(22)	Photolysis reaction
D3C106O2 + HO2 → D3C106OOH	KRO2HO2*0.914	
D3C106O2 + NO → D3C106NO3	KRO2NO*0.125	
D3C106O2 + NO → D3C106O + NO2	KRO2NO*0.875	
D3C106O2 + NO3 → D3C106O + NO2	KRO2NO3	
D3C106O2 → D3C106O	6.70E-15*0.7*RO2	
D3C106O2 → D3C106OH	6.70E-15*0.3*RO2	
D3C106OOH + OH → D3C106O2	8.01E-11	
D3C106OOH → D3C106O + OH	J(41)+J(15)	Photolysis reaction
D3C106NO3 + OH → CO235C6CHO + CH3COCH3 + NO2	7.03E-11	
D3C106NO3 → D3C106O + NO2	J(55)+J(15)	Photolysis reaction
D3C106O → C716O2 + CH3COCH3	KDEC	
D3C106OH + OH → D3C106O	7.66E-11	
D3C106OH → D3C106O + HO2	J(15)	Photolysis reaction

Table S6. Peroxy radical autoxidation mechanism (PRAM), monomer production. Rx (e.g. R1) in the 'Reactions' and 'Notes' columns corresponds to the reactions numbered in the main text.

Reactions	Rate constants (cm^3s^{-1})	Notes
D3CO2_O4i1 → D3CO2_O6i1	3E16*exp(-1.2077D4/TEMP)	0.075 s^{-1} at 298 K
D3CO2_O4i2 → D3CO2_O6i2	3E16*exp(-1.2077D4/TEMP)	0.075 s^{-1} at 298 K
D3CO2_O4i3 → D3CO2_O6i3	3E16*exp(-1.2077D4/TEMP)	0.075 s^{-1} at 298 K
D3CO2_C9_O4 → D3CO2_C9_O6	3E16*exp(-1.2077D4/TEMP)	0.075 s^{-1} at 298 K

D3CO2_O5i1 → D3CO2_O7i1	1E16*exp(-1.2077D4/TEMP)	0.025 s^{-1} at 298 K
D3CO2_O5i2 → D3CO2_O7i2	1E16*exp(-1.2077D4/TEMP)	0.025 s^{-1} at 298 K
D3CO2_O5i3 → D3CO2_O7i3	1E16*exp(-1.2077D4/TEMP)	0.025 s^{-1} at 298 K
D3CO2_C9_O5 → D3CO2_C9_O7	1E16*exp(-1.2077D4/TEMP)	0.025 s^{-1} at 298 K
D3CO2_O6i1 → D3CO2_O8i1	1E18*exp(-1.2077D4/TEMP)	2.5 s^{-1} at 298 K
D3CO2_O6i3 → D3CO2_O8i3	1E18*exp(-1.2077D4/TEMP)	2.5 s^{-1} at 298 K
D3CO2_C9_O6 → D3CO2_C9_O8	1E18*exp(-1.2077D4/TEMP)	2.5 s^{-1} at 298 K
D3CO2_O7i1 → D3CO2_O9i1	1E17*exp(-1.2077D4/TEMP)	0.25 s^{-1} at 298 K
D3CO2_O7i3 → D3CO2_O9i3	1E17*exp(-1.2077D4/TEMP)	0.25 s^{-1} at 298 K
D3CO2_O8i1 → D3CO2_O10i1	1E18*exp(-1.2077D4/TEMP)	2.5 s^{-1} at 298 K
D3CO2_C9_O8 → D3CO2_C9_O10	1E18*exp(-1.2077D4/TEMP)	2.5 s^{-1} at 298 K
D3CO2_O9i1 → D3CO2_O11i1	1E17*exp(-1.2077D4/TEMP)	0.25 s^{-1} at 298 K
D3CO2_O10i1 → D3CO2_O12	1E15*exp(-1.2077D4/TEMP)	0.0025 s^{-1} at 298 K
R1. Unimolecular termination RO_2 → R=O + OH		
D3CO2_O7i1 → D3CO6CBNiU1 + OH	0.0	R1
D3CO2_O7i2 → D3CO6CBNiU2 + OH	0.0	R1
D3CO2_O7i3 → D3CO6CBNiU3 + OH	0.0	R1
D3CO2_O8i1 → D3CO7CBNiU1 + OH	0.0	R1
D3CO2_O8i2 → D3CO7CBNiU2 + OH	0.0	R1
D3CO2_O8i3 → D3CO7CBNiU3 + OH	2E-2	R1 Based on COALA exp.
D3CO2_O9i1 → D3CO8CBNiU1 + OH	0.0	R1
D3CO2_O9i3 → D3CO8CBNiU3 + OH	2E-2	R1 Based on COALA exp.
D3CO2_O10i1 → D3CO9CBNiU1 + OH	2E-2	R1 Based on COALA exp.
D3CO2_O11i1 → D3CO10CBNiU1 + OH	0.0	R1
D3CO2_O12 → D3CO11CBNiU1 + OH	2E-2	R1 Based on COALA exp.
R11. Conversion of PRAM alkoxy radicals to peroxy radicals (RO + O_2 → RO_2)		
D3CO_O3i1 → D3CO2_O5i1	KDEC	R11
D3CO_O3i2 → D3CO2_O5i2	KDEC	R11
D3CO_O3i3 → D3CO2_O5i3	KDEC	R11
D3CO_C9_O3 → D3CO2_C9_O5	KDEC	R11
D3CO_O4i1 → D3CO2_O6i1	KDEC	R11
D3CO_O4i2 → D3CO2_O6i2	KDEC	R11
D3CO_O4i3 → D3CO2_O6i3	KDEC	R11
D3CO_C9_O4 → D3CO2_C9_O6	KDEC	R11
D3CO_O5i1 → D3CO2_O7i1	KDEC	R11
D3CO_O5i2 → D3CO2_O7i2	KDEC	R11
D3CO_O5i3 → D3CO2_O7i3	KDEC	R11
D3CO_C9_O5 → D3CO2_C9_O7	KDEC	R11
D3CO_O6i1 → D3CO2_O8i1	KDEC	R11
D3CO_O6i2 → D3CO2_O8i2	KDEC	R11

D3CO_O6i3 → D3CO2_O8i3	KDEC	R11
D3CO_C9_O6 → D3CO2_C9_O8	KDEC	R11
D3CO_O7i1 → D3CO2_O9i1	KDEC	R11
D3CO_O7i2 → D3CO2_O9i2	KDEC	R11
D3CO_O7i3 → D3CO2_O9i3	KDEC	R11
D3CO_C9_O7 → D3CO2_C9_O9	KDEC	R11
D3CO_O8i1 → D3CO2_O10i1	KDEC	R11
D3CO_C9_O8 → D3CO2_C9_O10	KDEC	R11
D3CO_O9i1 → D3CO2_O11i1	KDEC	R11
D3CO_O9i2 → D3CO2_O11i2	KDEC	R11
D3CO_O9i3 → D3CO2_O11i2	KDEC	R11
R6. $RO_2 + HO_2 \rightarrow ROOH + O_2$		
D3CO2_O4i1 + HO2 → D3CO4iH1	KRO2HO2	R6
D3CO2_O4i2 + HO2 → D3CO4iH2	KRO2HO2	R6
D3CO2_O4i3 + HO2 → D3CO4iH3	KRO2HO2	R6
D3CO2_C9_O4 + HO2 → D3C9O4	KRO2HO2	R6
D3CO2_O5i1 + HO2 → D3CO5iH1	KRO2HO2	R6
D3CO2_O5i2 + HO2 → D3CO5iH2	KRO2HO2	R6
D3CO2_O5i3 + HO2 → D3CO5iH3	KRO2HO2	R6
D3CO2_C9_O5 + HO2 → D3C9O5	KRO2HO2	R6
D3CO2_O6i1 + HO2 → D3CO6iH1	KRO2HO2	R6
D3CO2_O6i2 + HO2 → D3CO6iH2	KRO2HO2	R6
D3CO2_O6i3 + HO2 → D3CO6iH3	KRO2HO2	R6
D3CO2_C9_O6 + HO2 → D3C9O6	KRO2HO2	R6
D3CO2_O7i1 + HO2 → D3CO7iH1	KRO2HO2	R6
D3CO2_O7i2 + HO2 → D3CO7iH2	KRO2HO2	R6
D3CO2_O7i3 + HO2 → D3CO7iH3	KRO2HO2	R6
D3CO2_C9_O7 + HO2 → D3C9O7	KRO2HO2	R6
D3CO2_O8i1 + HO2 → D3CO8iH1	KRO2HO2	R6
D3CO2_O8i2 + HO2 → D3CO8iH2	KRO2HO2	R6
D3CO2_O8i3 + HO2 → D3CO8iH3	KRO2HO2	R6
D3CO2_C9_O8 + HO2 → D3C9O8	KRO2HO2	R6
D3CO2_O9i1 + HO2 → D3CO9iH1	KRO2HO2	R6
D3CO2_O9i2 + HO2 → D3CO9iH2	KRO2HO2	R6
D3CO2_O9i3 + HO2 → D3CO9iH3	KRO2HO2	R6
D3CO2_C9_O9 + HO2 → D3C9O9	KRO2HO2	R6
D3CO2_O10i1 + HO2 → D3CO10iH1	KRO2HO2*0.25	R6 Based on COALA CO exp.
D3CO2_O10i1 + HO2 → D3CO_O9iH1 + OH	KRO2HO2*0.75	R8 Based on COALA CO exp.
D3CO_O9iH1 → C511OOH+ CH3CO3 + HCOCH2CHO	KDEC	R10

D3CO2_C9_O10 + HO2 → D3C9O10	KRO2HO2	R6
D3CO2_O11i1 + HO2 → D3CO11iH1	KRO2HO2	R6
D3CO2_O11i2 + HO2 → D3CO11iH2	KRO2HO2	R6
D3CO2_O12 + HO2 → D3CO12iH	KRO2HO2	R6
R2, R3 & R5 RO_2 + RO_2 reactions leading to closed shell monomers and alkoxy radicals (RO)		
D3CO2_O4i1 → D3CO3CBNi1	1.2E-12*0.3*RO2	R3
D3CO2_O4i1 → D3CO_O3i1	1.2E-12*0.4*RO2	R2
D3CO2_O4i1 → D3CO3i1	1.2E-12*0.3*RO2	R3
D3CO2_O4i2 → D3CO3CBNi2	1.2E-12*0.3*RO2	R3
D3CO2_O4i2 → D3CO_O3i2	1.2E-12*0.4*RO2	R2
D3CO2_O4i2 → D3CO3i2	1.2E-12*0.3*RO2	R3
D3CO2_O4i3 → D3CO3CBNi3	1.2E-12*0.3*RO2	R3
D3CO2_O4i3 → D3CO_O3i3	1.2E-12*0.4*RO2	R2
D3CO2_O4i3 → D3CO3i3	1.2E-12*0.3*RO2	R3
D3CO2_C9_O4 → D3C9O3CBN	1.2E-12*0.3*RO2	R3
D3CO2_C9_O4 → D3CO_C9_O3	1.2E-12*0.4*RO2	R2
D3CO2_C9_O4 → D3C9O3	1.2E-12*0.3*RO2	R3
D3CO2_O5i1 → D3CO4CBNi1	1.2E-12*0.3*RO2	R3
D3CO2_O5i1 → D3CO_O4i1	1.2E-12*0.3*RO2	R2
D3CO2_O5i1 → D3CO4i1	1.2E-12*0.3*RO2	R3
D3CO2_O5i2 → D3CO4CBNi2	1.2E-12*0.3*RO2	R3
D3CO2_O5i2 → D3CO_O4i2	1.2E-12*0.4*RO2	R2
D3CO2_O5i2 → D3CO4i2	1.2E-12*0.3*RO2	R3
D3CO2_O5i3 → D3CO4CBNi3	1.2E-12*0.3*RO2	R3
D3CO2_O5i3 → D3CO_O4i3	1.2E-12*0.4*RO2	R2
D3CO2_O5i3 → D3CO4i3	1.2E-12*0.3*RO2	R3
D3CO2_C9_O5 → D3C9O4CBN	1.2E-12*0.3*RO2	R3
D3CO2_C9_O5 → D3CO_C9_O4	1.2E-12*0.4*RO2	R2
D3CO2_C9_O5 → D3C9O4	1.2E-12*0.3*RO2	R3
D3CO2_O6i1 → D3CO5CBNi1	1.6E-12*0.4*RO2	R3
D3CO2_O6i1 → D3CO_O5i1	1.6E-12*0.2*RO2	R2
D3CO2_O6i1 → D3CO5i1	1.6E-12*0.4*RO2	R3
D3CO2_O6i2 → D3CO5CBNi2	1.6E-12*0.4*RO2	R3
D3CO2_O6i2 → D3CO_O5i2	1.6E-12*0.2*RO2	R2
D3CO2_O6i2 → D3CO5i2	1.6E-12*0.4*RO2	R3
D3CO2_O6i3 → D3CO5CBNi3	1.6E-12*0.4*RO2	R3
D3CO2_O6i3 → D3CO_O5i3	1.6E-12*0.2*RO2	R2
D3CO2_O6i3 → D3CO5i3	1.6E-12*0.4*RO2	R3
D3CO2_C9_O6 → D3C9O6CBN	1.6E-12*0.4*RO2	R3
D3CO2_C9_O6 → D3CO_C9_O6	1.6E-12*0.2*RO2	R2

D3CO2_C9_O6 → D3C9O6	1.6E-12*0.4*RO2	R3
D3CO2_O7i1 → D3CO6CBNi1	2E-12*0.3*RO2	R3
D3CO2_O7i1 → D3CO_O6i1	2E-12*0.2*RO2	R2
D3CO2_O7i1 → D3CO6i1	2E-12*0.5*RO2	R3
D3CO2_O7i2 → D3CO6CBNi2	2E-12*0.3*RO2	R3
D3CO2_O7i2 → D3CO_O6i2	2E-12*0.2*RO2	R2
D3CO2_O7i2 → D3CO6i2	2E-12*0.5*RO2	R3
D3CO2_O7i3 → D3CO6CBNi3	2E-12*0.3*RO2	R3
D3CO2_O7i3 → D3CO_O6i3	2E-12*0.2*RO2	R2
D3CO2_O7i3 → D3CO6i3	2E-12*0.5*RO2	R3
D3CO2_C9_O7 → D3C9O6CBN	2E-12*0.3*RO2	R3
D3CO2_C9_O7 → D3CO_C9_O6	2E-12*0.2*RO2	R2
D3CO2_C9_O7 → D3C9O6	2E-12*0.5*RO2	R3
D3CO2_O8i1 → D3CO7CBNi1	2E-12*0.5*RO2	R3
D3CO2_O8i1 → D3CO_O7i1	2E-12*0.2*RO2	R2
D3CO2_O8i1 → D3CC7H8O7 + CH3COCH3	2E-12*0.0*RO2	R2 + R10
D3CO2_O8i1 → D3CO7i1	2E-12*0.3*RO2	R3
D3CO2_O8i2 → D3CO7CBNi2	2E-12*0.5*RO2	R3
D3CO2_O8i2 → D3CO_O7i2	2E-12*0.2*RO2	R2
D3CO2_O8i2 → D3CC7H8O7 + CH3COCH3	2E-12*0.0*RO2	R2 + R10
D3CO2_O8i2 → D3CO7i2	2E-12*0.3*RO2	R3
D3CO2_O8i3 → D3CO7CBNi3	2E-12*0.27*RO2	R3 Based on COALA exp
D3CO2_O8i3 → D3CO_O7i3	2E-12*0.2*RO2	R2
D3CO2_O8i3 → D3CC7H8O7 + CH3COCH3	2E-12*0.3*RO2	R2 + R10
D3CO2_O8i3 → D3CO7i3	2E-12*0.23*RO2	Based on COALA exp
D3CO2_C9_O8 → D3C9O7CBN	2E-12*0.5*RO2	R3
D3CO2_C9_O8 → D3CO_C9_O7	2E-12*0.2*RO2	R2
D3CO2_C9_O8 → D3C9O7	2E-12*0.3*RO2	R3
D3CO2_O9i1 → D3CO8CBNi1	2E-12*0.1*RO2	R3 Based on COALA exp
D3CO2_O9i1 → D3CC7H8O8 + CH3COCH3	2E-12*0.1*RO2	R2 + R10
D3CO2_O9i1 → D3CO8i1	2E-12*0.8*RO2	R3 Based on COALA exp
D3CO2_O9i2 → D3CO8CBNi2	2E-12*0.1*RO2	R3
D3CO2_O9i2 → D3CC7H8O8 + CH3COCH3	2E-12*0.1*RO2	R2 + R10
D3CO2_O9i2 → D3CO8i2	2E-12*0.8*RO2	R3
D3CO2_O9i3 → D3CO8CBNi3	2E-12*0.1*RO2	R3
D3CO2_O9i3 → D3CC7H8O8 + CH3COCH3	2E-12*0.1*RO2	R2 + R10
D3CO2_O9i3 → D3CO8i3	2E-12*0.8*RO2	R3
D3CO2_C9_O9 → D3C9O8CBN	2E-12*0.7*RO2	R3
D3CO2_C9_O9 → D3CO_C9_O8	2E-12*0.1*RO2	R2
D3CO2_C9_O9 → D3C9O8	2E-12*0.2*RO2	R3

D3CO2_O10i1 → D3CO9CBNi1	2E-12*0.55*RO2	R3 Based on COALA exp
D3CO2_O10i1 → D3CC7H8O8 + CH3COCH3	2E-12*0.0*RO2	R2 + R10
D3CO2_O10i1 → D3CO9iR1	2E-12*0.45*RO2	R3 Based on COALA exp
D3CO2_C9_O10 → D3C9O9CBN	2E-12*0.5*RO2	R3 Based on COALA exp
D3CO2_C9_O10 → D3C9O9	2E-12*0.5*RO2	R3 Based on COALA exp
D3CO2_O11i1 → D3CO10CBNi1	2E-12*0.2*RO2	R3
D3CO2_O11i1 → D3CC7H8O8 + CH3COCH3	2E-12*0.6*RO2	R2 + R10
D3CO2_O11i1 → D3CO10i1	2E-12*0.2*RO2	R3
D3CO2_O12 → D3CO11CBN	2E-12*0.8*RO2	R3
D3CO2_O12 → D3CC7H8O8 + CH3COCH3	2E-12*0.1*RO2	R2 + R10
D3CO2_O12 → D3CO11	2E-12*0.1*RO2	R3
Functionalization of PRAM RO_2 when they react with NO (RO_2 + NO →RO + NO_2)		
D3CO2_O4i1 + NO → D3CO_O3i1 + NO2	0.8*KRO2NO	
D3CO2_O4i2 + NO → D3CO_O3i2 + NO2	0.8*KRO2NO	
D3CO2_O4i3 + NO → D3CO_O3i3 + NO2	0.8*KRO2NO	
D3CO2_C9_O4 + NO → D3CO_C9_O3 + NO2	0.8*KRO2NO	
D3CO2_O5i1 + NO → D3CO_O4i1 + NO2	0.6*KRO2NO	
D3CO2_O5i2 + NO → D3CO_O4i2 + NO2	0.6*KRO2NO	
D3CO2_O5i3 + NO → D3CO_O4i3 + NO2	0.6*KRO2NO	
D3CO2_C9_O5 + NO → D3CO_C9_O4 + NO2	0.6*KRO2NO	
D3CO2_O6i1 + NO → D3CO_O5i1 + NO2	0.4*KRO2NO	
D3CO2_O6i2 + NO → D3CO_O5i2 + NO2	0.4*KRO2NO	
D3CO2_O6i3 + NO → D3CO_O5i3 + NO2	0.4*KRO2NO	
D3CO2_C9_O6 + NO → D3CO_C9_O5 + NO2	0.4*KRO2NO	
D3CO2_O7i1 + NO → D3CO_O6i1 + NO2	0.2*KRO2NO	
D3CO2_O7i2 + NO → D3CO_O6i2 + NO2	0.2*KRO2NO	
D3CO2_O7i3 + NO → D3CO_O6i3 + NO2	0.2*KRO2NO	
D3CO2_C9_O7 + NO → D3CO_C9_O6 + NO2	0.2*KRO2NO	
Fragmentation of RO_2 when they react with NO		
D3CO2_O4i1 + NO → C717O2 + CH3COCH3 + NO2	0.08*KRO2NO	
D3CO2_O4i2 + NO → C717O2 + CH3COCH3 + NO2	0.08*KRO2NO	
D3CO2_O4i3 + NO → C717O2 + CH3COCH3 + NO2	0.08*KRO2NO	
D3CO2_C9_O4 + NO → C717O2 + CH3CHO + NO2	0.08*KRO2NO	
D3CO2_O5i1 + NO → C717O2 + CH3COCH3+NO2	0.16*KRO2NO	
D3CO2_O5i2 + NO → C717O2 + CH3COCH3+NO2	0.16*KRO2NO	
D3CO2_O5i3 + NO → C717O2 + CH3COCH3+NO2	0.16*KRO2NO	
D3CO2_C9_O5 + NO → C717O2 + CH3CHO + NO2	0.16*KRO2NO	
D3CO2_O6i1 + NO → C717O2 + CH3COCH3 + NO2	0.24*KRO2NO	
D3CO2_O6i2 + NO → C717O2 + CH3COCH3 + NO2	0.24*KRO2NO	
D3CO2_O6i3 + NO → C717O2 + CH3COCH3 + NO2	0.24*KRO2NO	

D3CO2_C9_O6 + NO → C717O2 + CH3CHO + NO2	0.24*KRO2NO
D3CO2_O7i1 + NO → C717O2 + CH3COCH3+NO2	0.32*KRO2NO
D3CO2_O7i2 + NO → C717O2 + CH3COCH3+NO2	0.32*KRO2NO
D3CO2_O7i3 + NO → C717O2 + CH3COCH3+NO2	0.32*KRO2NO
D3CO2_C9_O7 + NO → C717O2 + CH3CHO + NO2	0.32*KRO2NO
D3CO2_O8i1 + NO → D3CC7H8O7 + CH3COCH3+NO2	0.4*KRO2NO
D3CO2_O8i2 + NO → D3CC7H8O7 + CH3COCH3+NO2	0.4*KRO2NO
D3CO2_O8i3 + NO → D3CC7H8O7 + CH3COCH3+NO2	0.4*KRO2NO
D3CO2_C9_O8 + NO → D3CC7H8O7 + CH3CHO + NO2	0.4*KRO2NO
D3CO2_O9i1 + NO → R_C7H11O7 + MGLYOX+NO2	0.4*KRO2NO
D3CO2_O9i2 + NO → R_C7H11O7 + MGLYOX+NO2	0.4*KRO2NO
D3CO2_O9i3 + NO → R_C7H11O7 + MGLYOX+NO2	0.4*KRO2NO
D3CO2_C9_O9 + NO → R_C7H11O7 + GLYOX + NO2	0.4*KRO2NO
D3CO2_O10i1 + NO → R_C7H11O7 + CH3COCO2H+NO2	0.4*KRO2NO
D3CO2_C9_O10 + NO → R_C7H11O7 + GLYOX + NO2	0.4*KRO2NO
D3CO2_O11i1 + NO → D3CC7H8O8 + CH3COCH3+NO2	0.4*KRO2NO
D3CO2_O11i2 + NO → D3CC7H8O8 + CH3COCH3+NO2	0.4*KRO2NO
D3CO2_O12 + NO → D3CC7H8O8 + CH3COCH3+NO2	0.4*KRO2NO
R_C7H11O7 + NO → D3CC7NO3_O8	KRO2NO
R_C7H11O7 → D3CC7H10O6	5.0E-12*RO2
RO_2 + NO → R→O + NO_2 + HO_2	
D3CO2_O4i1 + NO → D3CO3CBNi1 + NO2 + HO2	0.06*KRO2NO
D3CO2_O4i2 + NO → D3CO3CBNi2 + NO2 + HO2	0.06*KRO2NO
D3CO2_O4i3 + NO → D3CO3CBNi3 + NO2 + HO2	0.06*KRO2NO
D3CO2_C9_O4 + NO → D3C9O3CBN + NO2 + HO2	0.06*KRO2NO
D3CO2_O5i1 + NO → D3CO4CBNi1 + NO2 + HO2	0.12*KRO2NO
D3CO2_O5i2 + NO → D3CO4CBNi2 + NO2 + HO2	0.12*KRO2NO
D3CO2_O5i3 + NO → D3CO4CBNi3 + NO2 + HO2	0.12*KRO2NO
D3CO2_C9_O5 + NO → D3C9O4CBN + NO2 + HO2	0.12*KRO2NO
D3CO2_O6i1 + NO → D3CO5CBNi1 + NO2 + HO2	0.18*KRO2NO
D3CO2_O6i2 + NO → D3CO5CBNi2 + NO2 + HO2	0.18*KRO2NO
D3CO2_O6i3 + NO → D3CO5CBNi3 + NO2 + HO2	0.18*KRO2NO
D3CO2_C9_O6 + NO → D3C9O5CBN + NO2 + HO2	0.18*KRO2NO
D3CO2_O7i1 + NO → D3CO6CBNi1 + NO2 + HO2	0.24*KRO2NO
D3CO2_O7i2 + NO → D3CO6CBNi2 + NO2 + HO2	0.24*KRO2NO
D3CO2_O7i3 + NO → D3CO6CBNi3 + NO2 + HO2	0.24*KRO2NO

D3CO2_C9_O7 + NO → D3C9O6CBN + NO2 + HO2	0.24*KRO2NO
D3CO2_O8i1 + NO → D3CO7CBNi1 + NO2 + HO2	0.3*KRO2NO
D3CO2_O8i2 + NO → D3CO7CBNi2 + NO2 + HO2	0.3*KRO2NO
D3CO2_O8i3 + NO → D3CO7CBNi3 + NO2 + HO2	0.3*KRO2NO
D3CO2_C9_O8 + NO → D3C9O7CBN + NO2 + HO2	0.3*KRO2NO
D3CO2_O9i1 + NO → D3CO8CBNi1 + NO2 + HO2	0.3*KRO2NO
D3CO2_O9i2 + NO → D3CO8CBNi2 + NO2 + HO2	0.3*KRO2NO
D3CO2_O9i3 + NO → D3CO8CBNi3 + NO2 + HO2	0.3*KRO2NO
D3CO2_C9_O9 + NO → D3C9O8CBN + NO2 + HO2	0.3*KRO2NO
D3CO2_O10i1 + NO → D3CO9CBNi1 + NO2 + HO2	0.3*KRO2NO
D3CO2_C9_O10 + NO → D3C9O9CBN + NO2 + HO2	0.3*KRO2NO
D3CO2_O11i1 + NO → D3CO10CBNi1 + NO2 + HO2	0.3*KRO2NO
D3CO2_O11i2 + NO → D3CO10CBNi2 + NO2 + HO2	0.3*KRO2NO
D3CO2_O12 + NO → D3CO11CBN + NO2 + HO2	0.3*KRO2NO
RO_2 + NO → R-NO_3	
D3CO2_O4i1 + NO → D3CNO5i1	0.06*KRO2NO
D3CO2_O4i2 + NO → D3CNO5i2	0.06*KRO2NO
D3CO2_O4i3 + NO → D3CNO5i3	0.06*KRO2NO
D3CO2_C9_O4 + NO → D3C9NO5	0.06*KRO2NO
D3CO2_O5i1 + NO → D3CNO6i1	0.12*KRO2NO
D3CO2_O5i2 + NO → D3CNO6i2	0.12*KRO2NO
D3CO2_O5i3 + NO → D3CNO6i3	0.12*KRO2NO
D3CO2_C9_O5 + NO → D3C9NO6	0.12*KRO2NO
D3CO2_O6i1 + NO → D3CNO7i1	0.18*KRO2NO
D3CO2_O6i2 + NO → D3CNO7i2	0.18*KRO2NO
D3CO2_O6i3 + NO → D3CNO7i3	0.18*KRO2NO
D3CO2_C9_O6 + NO → D3C9NO7	0.18*KRO2NO
D3CO2_O7i1 + NO → D3CNO8i1	0.24*KRO2NO
D3CO2_O7i2 + NO → D3CNO8i2	0.24*KRO2NO
D3CO2_O7i3 + NO → D3CNO8i3	0.24*KRO2NO
D3CO2_C9_O7 + NO → D3C9NO8	0.24*KRO2NO
D3CO2_O8i1 + NO → D3CNO9i1	0.3*KRO2NO
D3CO2_O8i2 + NO → D3CNO9i2	0.3*KRO2NO
D3CO2_O8i3 + NO → D3CNO9i3	0.3*KRO2NO
D3CO2_C9_O8 + NO → D3C9NO9	0.3*KRO2NO
D3CO2_O9i1 + NO → D3CNO10i1	0.3*KRO2NO
D3CO2_O9i2 + NO → D3CNO10i2	0.3*KRO2NO
D3CO2_O9i3 + NO → D3CNO10i3	0.3*KRO2NO
D3CO2_C9_O9 + NO → D3C9NO10	0.3*KRO2NO
D3CO2_O10i1 + NO → D3CNO11i1	0.3*KRO2NO

D3CO2_C9_O10 + NO → D3C9NO11	0.3*KRO2NO
D3CO2_O11i1 + NO → D3CNO12i1	0.3*KRO2NO
D3CO2_O11i2 + NO → D3CNO12i2	0.3*KRO2NO
D3CO2_O12 + NO → D3CNO13	0.3*KRO2NO

Table S7. Peroxy radical autoxidation mechanism (PRAM), dimer production. Rx (e.g. R1) in the 'Notes' column corresponds to the reactions numbered in the main text.

Reactions	Rate constants ($cm^3 s^{-1}$)	Notes
D3C1O2+D3CO2_O4i1 → D3C20H32_O5	1E-13	R4
D3C2O2+D3CO2_O4i1 → D3C20H32_O5	1E-13	R4
D3C96CO3+D3CO2_O4i1 → D3C20H30_O6	1E-13	R4
D3CALO2+D3CO2_O4i1 → D3C20H30_O6	1E-13	R4
D3C106O2+D3CO2_O4i1 → D3C20H30_O7	1E-13	R4
D3C107O2+D3CO2_O4i1 → D3C20H30_O6	1E-13	R4
D3C108O2+D3CO2_O4i1 → D3C20H30_O7	1E-13	R4
D3C109O2+D3CO2_O4i1 → D3C20H30_O6	1E-13	R4
D3C920CO3+D3CO2_O4i1 → D3C20H30_O7	1E-13	R4
D3C96O2+D3CO2_O4i1 → D3C19H30_O5	1E-13	R4
D3C89CO3+D3CO2_O4i1 → D3C19H28_O6	1E-13	R4
D3C920O2+D3CO2_O4i1 → D3C19H30_O6	1E-13	R4
D3C811CO3+D3CO2_O4i1 → D3C19H28_O7	1E-13	R4
D3C921O2+D3CO2_O4i1 → D3C19H30_O7	1E-13	R4
D3C922O2+D3CO2_O4i1 → D3C19H30_O8	1E-13	R4
D3C97O2+D3CO2_O4i1 → D3C19H30_O6	1E-13	R4
D3C98O2+D3CO2_O4i1 → D3C19H30_O7	1E-13	R4
D3C89O2+D3CO2_O4i1 → D3C18H28_O5	1E-13	R4
D3C810O2+D3CO2_O4i1 → D3C18H28_O6	1E-13	R4
D3C811O2+D3CO2_O4i1 → D3C18H28_O6	1E-13	R4
D3C812O2+D3CO2_O4i1 → D3C18H28_O7	1E-13	R4
D3C813O2+D3CO2_O4i1 → D3C18H28_O8	1E-13	R4
D3C85O2+D3CO2_O4i1 → D3C18H28_O5	1E-13	R4
D3C86O2+D3CO2_O4i1 → D3C18H28_O6	1E-13	R4
D3C721CO3+D3CO2_O4i1 → D3C18H26_O7	1E-13	R4
D3C1O2+D3CO2_O4i2 → D3C20H30_O5	1E-13	R4
D3C2O2+D3CO2_O4i2 → D3C20H30_O5	1E-13	R4
D3C96CO3+D3CO2_O4i2 → D3C20H30_O6	1E-13	R4
D3CALO2+D3CO2_O4i2 → D3C20H30_O6	1E-13	R4
D3C106O2+D3CO2_O4i2 → D3C20H30_O7	1E-13	R4

D3C107O2+D3CO2_O4i2 → D3C20H30_O6	1E-13	R4
D3C108O2+D3CO2_O4i2 → D3C20H30_O7	1E-13	R4
D3C109O2+D3CO2_O4i2 → D3C20H30_O6	1E-13	R4
D3C920CO3+D3CO2_O4i2 → D3C20H30_O7	1E-13	R4
D3C96O2+D3CO2_O4i2 → D3C19H30_O5	1E-13	R4
D3C89CO3+D3CO2_O4i2 → D3C19H28_O6	1E-13	R4
D3C920O2+D3CO2_O4i2 → D3C19H30_O6	1E-13	R4
D3C811CO3+D3CO2_O4i2 → D3C19H28_O7	1E-13	R4
D3C921O2+D3CO2_O4i2 → D3C19H30_O7	1E-13	R4
D3C922O2+D3CO2_O4i2 → D3C19H30_O8	1E-13	R4
D3C97O2+D3CO2_O4i2 → D3C19H30_O6	1E-13	R4
D3C98O2+D3CO2_O4i2 → D3C19H30_O7	1E-13	R4
D3C89O2+D3CO2_O4i2 → D3C18H28_O5	1E-13	R4
D3C810O2+D3CO2_O4i2 → D3C18H28_O6	1E-13	R4
D3C811O2+D3CO2_O4i2 → D3C18H28_O6	1E-13	R4
D3C812O2+D3CO2_O4i2 → D3C18H28_O7	1E-13	R4
D3C813O2+D3CO2_O4i2 → D3C18H28_O8	1E-13	R4
D3C85O2+D3CO2_O4i2 → D3C18H28_O5	1E-13	R4
D3C86O2+D3CO2_O4i2 → D3C18H28_O6	1E-13	R4
D3C721CO3+D3CO2_O4i2 → D3C18H26_O7	1E-13	R4
D3C1O2+D3CO2_O4i3 → D3C20H32_O5	1E-13	R4
D3C2O2+D3CO2_O4i3 → D3C20H32_O5	1E-13	R4
D3C96CO3+D3CO2_O4i3 → D3C20H30_O6	1E-13	R4
D3CALO2+D3CO2_O4i3 → D3C20H30_O6	1E-13	R4
D3C106O2+D3CO2_O4i3 → D3C20H30_O7	1E-13	R4
D3C107O2+D3CO2_O4i3 → D3C20H30_O6	1E-13	R4
D3C108O2+D3CO2_O4i3 → D3C20H30_O7	1E-13	R4
D3C109O2+D3CO2_O4i3 → D3C20H30_O6	1E-13	R4
D3C920CO3+D3CO2_O4i3 → D3C20H30_O7	1E-13	R4
D3C96O2+D3CO2_O4i3 → D3C19H30_O5	1E-13	R4
D3C89CO3+D3CO2_O4i3 → D3C19H28_O6	1E-13	R4
D3C920O2+D3CO2_O4i3 → D3C19H30_O6	1E-13	R4
D3C811CO3+D3CO2_O4i3 → D3C19H28_O7	1E-13	R4
D3C921O2+D3CO2_O4i3 → D3C19H30_O7	1E-13	R4
D3C922O2+D3CO2_O4i3 → D3C19H30_O8	1E-13	R4
D3C97O2+D3CO2_O4i3 → D3C19H30_O6	1E-13	R4
D3C98O2+D3CO2_O4i3 → D3C19H30_O7	1E-13	R4
D3C89O2+D3CO2_O4i3 → D3C18H28_O5	1E-13	R4
D3C810O2+D3CO2_O4i3 → D3C18H28_O6	1E-13	R4

D3C811O2+D3CO2_O4i3 → D3C18H28_O6	1E-13	R4
D3C812O2+D3CO2_O4i3 → D3C18H28_O7	1E-13	R4
D3C813O2+D3CO2_O4i3 → D3C18H28_O8	1E-13	R4
D3C85O2+D3CO2_O4i3 → D3C18H28_O5	1E-13	R4
D3C86O2+D3CO2_O4i3 → D3C18H28_O6	1E-13	R4
D3C721CO3+D3CO2_O4i3 → D3C18H26_O7	1E-13	R4
D3C1O2+D3CO2_C9_O4 → D3C19H30_O5	1E-13	R4
D3C2O2+D3CO2_C9_O4 → D3C19H30_O5	1E-13	R4
D3C96CO3+D3CO2_C9_O4 → D3C19H28_O6	1E-13	R4
D3CALO2+D3CO2_C9_O4 → D3C19H28_O6	1E-13	R4
D3C106O2+D3CO2_C9_O4 → D3C19H28_O7	1E-13	R4
D3C107O2+D3CO2_C9_O4 → D3C19H28_O6	1E-13	R4
D3C108O2+D3CO2_C9_O4 → D3C19H28_O7	1E-13	R4
D3C109O2+D3CO2_C9_O4 → D3C19H28_O6	1E-13	R4
D3C920CO3+D3CO2_C9_O4 → D3C19H28_O7	1E-13	R4
D3C96O2+D3CO2_C9_O4 → D3C18H28_O5	1E-13	R4
D3C89CO3+D3CO2_C9_O4 → D3C18H26_O6	1E-13	R4
D3C920O2+D3CO2_C9_O4 → D3C18H28_O6	1E-13	R4
D3C811CO3+D3CO2_C9_O4 → D3C18H26_O7	1E-13	R4
D3C921O2+D3CO2_C9_O4 → D3C18H28_O7	1E-13	R4
D3C922O2+D3CO2_C9_O4 → D3C18H28_O8	1E-13	R4
D3C97O2+D3CO2_C9_O4 → D3C18H28_O6	1E-13	R4
D3C98O2+D3CO2_C9_O4 → D3C18H28_O7	1E-13	R4
D3C89O2+D3CO2_C9_O4 → D3C17H26_O5	1E-13	R4
D3C810O2+D3CO2_C9_O4 → D3C17H26_O6	1E-13	R4
D3C811O2+D3CO2_C9_O4 → D3C17H26_O6	1E-13	R4
D3C812O2+D3CO2_C9_O4 → D3C17H26_O7	1E-13	R4
D3C813O2+D3CO2_C9_O4 → D3C17H26_O8	1E-13	R4
D3C85O2+D3CO2_C9_O4 → D3C17H26_O5	1E-13	R4
D3C86O2+D3CO2_C9_O4 → D3C17H26_O6	1E-13	R4
D3C721CO3+D3CO2_C9_O4 → D3C17H24_O7	1E-13	R4
D3C1O2+D3CO2_O5i1 → D3C20H32_O6	2E-13	R4
D3C2O2+D3CO2_O5i1 → D3C20H32_O6	2E-13	R4
D3C96CO3+D3CO2_O5i1 → D3C20H30_O7	2E-13	R4
D3CALO2+D3CO2_O5i1 → D3C20H30_O7	2E-13	R4
D3C106O2+D3CO2_O5i1 → D3C20H30_O8	2E-13	R4
D3C107O2+D3CO2_O5i1 → D3C20H30_O7	2E-13	R4
D3C108O2+D3CO2_O5i1 → D3C20H30_O8	2E-13	R4

D3C109O2+D3CO2_O5i1 → D3C20H30_O7	2E-13	R4
D3C920CO3+D3CO2_O5i1 → D3C20H30_O8	2E-13	R4
D3C96O2+D3CO2_O5i1 → D3C19H30_O6	2E-13	R4
D3C89CO3+D3CO2_O5i1 → D3C19H28_O7	2E-13	R4
D3C920O2+D3CO2_O5i1 → D3C19H30_O7	2E-13	R4
D3C811CO3+D3CO2_O5i1 → D3C19H28_O8	2E-13	R4
D3C921O2+D3CO2_O5i1 → D3C19H30_O8	2E-13	R4
D3C922O2+D3CO2_O5i1 → D3C19H30_O9	2E-13	R4
D3C97O2+D3CO2_O5i1 → D3C19H30_O7	2E-13	R4
D3C98O2+D3CO2_O5i1 → D3C19H30_O8	2E-13	R4
D3C89O2+D3CO2_O5i1 → D3C18H28_O6	2E-13	R4
D3C810O2+D3CO2_O5i1 → D3C18H28_O7	2E-13	R4
D3C811O2+D3CO2_O5i1 → D3C18H28_O7	2E-13	R4
D3C812O2+D3CO2_O5i1 → D3C18H28_O8	2E-13	R4
D3C813O2+D3CO2_O5i1 → D3C18H28_O9	2E-13	R4
D3C85O2+D3CO2_O5i1 → D3C18H28_O6	2E-13	R4
D3C86O2+D3CO2_O5i1 → D3C18H28_O7	2E-13	R4
D3C721CO3+D3CO2_O5i1 → D3C18H26_O8	2E-13	R4
D3C1O2+D3CO2_O5i2 → D3C20H32_O6	2E-13	R4
D3C2O2+D3CO2_O5i2 → D3C20H32_O6	2E-13	R4
D3C96CO3+D3CO2_O5i2 → D3C20H30_O7	2E-13	R4
D3CALO2+D3CO2_O5i2 → D3C20H30_O7	2E-13	R4
D3C106O2+D3CO2_O5i2 → D3C20H30_O8	2E-13	R4
D3C107O2+D3CO2_O5i2 → D3C20H30_O7	2E-13	R4
D3C108O2+D3CO2_O5i2 → D3C20H30_O8	2E-13	R4
D3C109O2+D3CO2_O5i2 → D3C20H30_O7	2E-13	R4
D3C920CO3+D3CO2_O5i2 → D3C20H30_O8	2E-13	R4
D3C96O2+D3CO2_O5i2 → D3C19H30_O6	2E-13	R4
D3C89CO3+D3CO2_O5i2 → D3C19H28_O7	2E-13	R4
D3C920O2+D3CO2_O5i2 → D3C19H30_O7	2E-13	R4
D3C811CO3+D3CO2_O5i2 → D3C19H28_O8	2E-13	R4
D3C921O2+D3CO2_O5i2 → D3C19H30_O8	2E-13	R4
D3C922O2+D3CO2_O5i2 → D3C19H30_O9	2E-13	R4
D3C97O2+D3CO2_O5i2 → D3C19H30_O7	2E-13	R4
D3C98O2+D3CO2_O5i2 → D3C19H30_O8	2E-13	R4
D3C89O2+D3CO2_O5i2 → D3C18H28_O6	2E-13	R4
D3C810O2+D3CO2_O5i2 → D3C18H28_O7	2E-13	R4
D3C811O2+D3CO2_O5i2 → D3C18H28_O7	2E-13	R4
D3C812O2+D3CO2_O5i2 → D3C18H28_O8	2E-13	R4

D3C813O2+D3CO2_O5i2 → D3C18H28_O9	2E-13	R4
D3C85O2+D3CO2_O5i2 → D3C18H28_O6	2E-13	R4
D3C86O2+D3CO2_O5i2 → D3C18H28_O7	2E-13	R4
D3C721CO3+D3CO2_O5i2 → D3C18H26_O8	2E-13	R4
D3C1O2+D3CO2_O5i3 → D3C20H32_O6	2E-13	R4
D3C2O2+D3CO2_O5i3 → D3C20H32_O6	2E-13	R4
D3C96CO3+D3CO2_O5i3 → D3C20H30_O7	2E-13	R4
D3CALO2+D3CO2_O5i3 → D3C20H30_O7	2E-13	R4
D3C106O2+D3CO2_O5i3 → D3C20H30_O8	2E-13	R4
D3C107O2+D3CO2_O5i3 → D3C20H30_O7	2E-13	R4
D3C108O2+D3CO2_O5i3 → D3C20H30_O8	2E-13	R4
D3C109O2+D3CO2_O5i3 → D3C20H30_O7	2E-13	R4
D3C920CO3+D3CO2_O5i3 → D3C20H30_O8	2E-13	R4
D3C96O2+D3CO2_O5i3 → D3C19H30_O6	2E-13	R4
D3C89CO3+D3CO2_O5i3 → D3C19H28_O7	2E-13	R4
D3C920O2+D3CO2_O5i3 → D3C19H30_O7	2E-13	R4
D3C811CO3+D3CO2_O5i3 → D3C19H28_O8	2E-13	R4
D3C921O2+D3CO2_O5i3 → D3C19H30_O8	2E-13	R4
D3C922O2+D3CO2_O5i3 → D3C19H30_O9	2E-13	R4
D3C97O2+D3CO2_O5i3 → D3C19H30_O7	2E-13	R4
D3C98O2+D3CO2_O5i3 → D3C19H30_O8	2E-13	R4
D3C89O2+D3CO2_O5i3 → D3C18H28_O6	2E-13	R4
D3C810O2+D3CO2_O5i3 → D3C18H28_O7	2E-13	R4
D3C811O2+D3CO2_O5i3 → D3C18H28_O7	2E-13	R4
D3C812O2+D3CO2_O5i3 → D3C18H28_O8	2E-13	R4
D3C813O2+D3CO2_O5i3 → D3C18H28_O9	2E-13	R4
D3C85O2+D3CO2_O5i3 → D3C18H28_O6	2E-13	R4
D3C86O2+D3CO2_O5i3 → D3C18H28_O7	2E-13	R4
D3C721CO3+D3CO2_O5i3 → D3C18H26_O8	2E-13	R4
D3C1O2+D3CO2_C9_O5 → D3C19H30_O6	2E-13	R4
D3C2O2+D3CO2_C9_O5 → D3C19H30_O6	2E-13	R4
D3C96CO3+D3CO2_C9_O5 → D3C19H28_O7	2E-13	R4
D3CALO2+D3CO2_C9_O5 → D3C19H28_O7	2E-13	R4
D3C106O2+D3CO2_C9_O5 → D3C19H28_O8	2E-13	R4
D3C107O2+D3CO2_C9_O5 → D3C19H28_O7	2E-13	R4
D3C108O2+D3CO2_C9_O5 → D3C19H28_O8	2E-13	R4
D3C109O2+D3CO2_C9_O5 → D3C19H28_O7	2E-13	R4
D3C920CO3+D3CO2_C9_O5 → D3C19H28_O8	2E-13	R4

D3C96O2+D3CO2_C9_O5 → D3C18H28_O6	2E-13	R4
D3C89CO3+D3CO2_C9_O5 → D3C18H26_O7	2E-13	R4
D3C920O2+D3CO2_C9_O5 → D3C18H28_O7	2E-13	R4
D3C811CO3+D3CO2_C9_O5 → D3C18H26_O8	2E-13	R4
D3C921O2+D3CO2_C9_O5 → D3C18H28_O8	2E-13	R4
D3C922O2+D3CO2_C9_O5 → D3C18H28_O9	2E-13	R4
D3C97O2+D3CO2_C9_O5 → D3C18H28_O7	2E-13	R4
D3C98O2+D3CO2_C9_O5 → D3C18H28_O8	2E-13	R4
D3C89O2+D3CO2_C9_O5 → D3C17H26_O6	2E-13	R4
D3C810O2+D3CO2_C9_O5 → D3C17H26_O7	2E-13	R4
D3C811O2+D3CO2_C9_O5 → D3C17H26_O7	2E-13	R4
D3C812O2+D3CO2_C9_O5 → D3C17H26_O8	2E-13	R4
D3C813O2+D3CO2_C9_O5 → D3C17H26_O9	2E-13	R4
D3C85O2+D3CO2_C9_O5 → D3C17H26_O6	2E-13	R4
D3C86O2+D3CO2_C9_O5 → D3C17H26_O7	2E-13	R4
D3C721CO3+D3CO2_C9_O5 → D3C17H24_O8	2E-13	R4
D3C1O2+D3CO2_O6i1 → D3C20H32_O7	1.2E-12	R4
D3C2O2+D3CO2_O6i1 → D3C20H32_O7	1.2E-12	R4
D3C96CO3+D3CO2_O6i1 → D3C20H30_O8	1.2E-12	R4
D3CALO2+D3CO2_O6i1 → D3C20H30_O8	1.2E-12	R4
D3C106O2+D3CO2_O6i1 → D3C20H30_O9	1.2E-12	R4
D3C107O2+D3CO2_O6i1 → D3C20H30_O8	1.2E-12	R4
D3C108O2+D3CO2_O6i1 → D3C20H30_O9	1.2E-12	R4
D3C109O2+D3CO2_O6i1 → D3C20H30_O8	1.2E-12	R4
D3C920CO3+D3CO2_O6i1 → D3C20H30_O9	1.2E-12	R4
D3C96O2+D3CO2_O6i1 → D3C19H30_O7	1.2E-12	R4
D3C89CO3+D3CO2_O6i1 → D3C19H28_O8	1.2E-12	R4
D3C920O2+D3CO2_O6i1 → D3C19H30_O8	1.2E-12	R4
D3C811CO3+D3CO2_O6i1 → D3C19H28_O9	1.2E-12	R4
D3C921O2+D3CO2_O6i1 → D3C19H30_O9	1.2E-12	R4
D3C922O2+D3CO2_O6i1 → D3C19H30_O10	1.2E-12	R4
D3C97O2+D3CO2_O6i1 → D3C19H30_O8	1.2E-12	R4
D3C98O2+D3CO2_O6i1 → D3C19H30_O9	1.2E-12	R4
D3C89O2+D3CO2_O6i1 → D3C18H28_O7	1.2E-12	R4
D3C810O2+D3CO2_O6i1 → D3C18H28_O8	1.2E-12	R4
D3C811O2+D3CO2_O6i1 → D3C18H28_O8	1.2E-12	R4
D3C812O2+D3CO2_O6i1 → D3C18H28_O9	1.2E-12	R4
D3C813O2+D3CO2_O6i1 → D3C18H28_O10	1.2E-12	R4
D3C85O2+D3CO2_O6i1 → D3C18H28_O7	1.2E-12	R4

D3C86O2+D3CO2_O6i1 → D3C18H28_O8	1.2E-12	R4
D3C721CO3+D3CO2_O6i1 → D3C18H26_O9	1.2E-12	R4
D3C1O2+D3CO2_O6i2 → D3C20H32_O7	1.2E-12	R4
D3C2O2+D3CO2_O6i2 → D3C20H32_O7	1.2E-12	R4
D3C96CO3+D3CO2_O6i2 → D3C20H30_O8	1.2E-12	R4
D3CALO2+D3CO2_O6i2 → D3C20H30_O8	1.2E-12	R4
D3C106O2+D3CO2_O6i2 → D3C20H30_O9	1.2E-12	R4
D3C107O2+D3CO2_O6i2 → D3C20H30_O8	1.2E-12	R4
D3C108O2+D3CO2_O6i2 → D3C20H30_O9	1.2E-12	R4
D3C109O2+D3CO2_O6i2 → D3C20H30_O8	1.2E-12	R4
D3C920CO3+D3CO2_O6i2 → D3C20H30_O9	1.2E-12	R4
D3C96O2+D3CO2_O6i2 → D3C19H30_O7	1.2E-12	R4
D3C89CO3+D3CO2_O6i2 → D3C19H28_O8	1.2E-12	R4
D3C920O2+D3CO2_O6i2 → D3C19H30_O8	1.2E-12	R4
D3C811CO3+D3CO2_O6i2 → D3C19H28_O9	1.2E-12	R4
D3C921O2+D3CO2_O6i2 → D3C19H30_O9	1.2E-12	R4
D3C922O2+D3CO2_O6i2 → D3C19H30_O10	1.2E-12	R4
D3C97O2+D3CO2_O6i2 → D3C19H30_O8	1.2E-12	R4
D3C98O2+D3CO2_O6i2 → D3C19H30_O9	1.2E-12	R4
D3C89O2+D3CO2_O6i2 → D3C18H28_O7	1.2E-12	R4
D3C810O2+D3CO2_O6i2 → D3C18H28_O8	1.2E-12	R4
D3C811O2+D3CO2_O6i2 → D3C18H28_O8	1.2E-12	R4
D3C812O2+D3CO2_O6i2 → D3C18H28_O9	1.2E-12	R4
D3C813O2+D3CO2_O6i2 → D3C18H28_O10	1.2E-12	R4
D3C85O2+D3CO2_O6i2 → D3C18H28_O7	1.2E-12	R4
D3C86O2+D3CO2_O6i2 → D3C18H28_O8	1.2E-12	R4
D3C721CO3+D3CO2_O6i2 → D3C18H26_O9	1.2E-12	R4
D3C1O2+D3CO2_O6i3 → D3C20H32_O7	1.2E-12	R4
D3C2O2+D3CO2_O6i3 → D3C20H32_O7	1.2E-12	R4
D3C96CO3+D3CO2_O6i3 → D3C20H30_O8	1.2E-12	R4
D3CALO2+D3CO2_O6i3 → D3C20H30_O8	1.2E-12	R4
D3C106O2+D3CO2_O6i3 → D3C20H30_O9	1.2E-12	R4
D3C107O2+D3CO2_O6i3 → D3C20H30_O8	1.2E-12	R4
D3C108O2+D3CO2_O6i3 → D3C20H30_O9	1.2E-12	R4
D3C109O2+D3CO2_O6i3 → D3C20H30_O8	1.2E-12	R4
D3C920CO3+D3CO2_O6i3 → D3C20H30_O9	1.2E-12	R4
D3C96O2+D3CO2_O6i3 → D3C19H30_O7	1.2E-12	R4
D3C89CO3+D3CO2_O6i3 → D3C19H28_O8	1.2E-12	R4

D3C920O2+D3CO2_O6i3 → D3C19H30_O8	1.2E-12	R4
D3C811CO3+D3CO2_O6i3 → D3C19H28_O9	1.2E-12	R4
D3C921O2+D3CO2_O6i3 → D3C19H30_O9	1.2E-12	R4
D3C922O2+D3CO2_O6i3 → D3C19H30_O10	1.2E-12	R4
D3C97O2+D3CO2_O6i3 → D3C19H30_O8	1.2E-12	R4
D3C98O2+D3CO2_O6i3 → D3C19H30_O9	1.2E-12	R4
D3C89O2+D3CO2_O6i3 → D3C18H28_O7	1.2E-12	R4
D3C810O2+D3CO2_O6i3 → D3C18H28_O8	1.2E-12	R4
D3C811O2+D3CO2_O6i3 → D3C18H28_O8	1.2E-12	R4
D3C812O2+D3CO2_O6i3 → D3C18H28_O9	1.2E-12	R4
D3C813O2+D3CO2_O6i3 → D3C18H28_O10	1.2E-12	R4
D3C85O2+D3CO2_O6i3 → D3C18H28_O7	1.2E-12	R4
D3C86O2+D3CO2_O6i3 → D3C18H28_O8	1.2E-12	R4
D3C721CO3+D3CO2_O6i3 → D3C18H26_O9	1.2E-12	R4
D3C1O2+D3CO2_C9_O6 → D3C19H30_O7	1.2E-12	R4
D3C2O2+D3CO2_C9_O6 → D3C19H30_O7	1.2E-12	R4
D3C96CO3+D3CO2_C9_O6 → D3C19H28_O8	1.2E-12	R4
D3CALO2+D3CO2_C9_O6 → D3C19H28_O8	1.2E-12	R4
D3C106O2+D3CO2_C9_O6 → D3C19H28_O9	1.2E-12	R4
D3C107O2+D3CO2_C9_O6 → D3C19H28_O8	1.2E-12	R4
D3C108O2+D3CO2_C9_O6 → D3C19H28_O9	1.2E-12	R4
D3C109O2+D3CO2_C9_O6 → D3C19H28_O8	1.2E-12	R4
D3C920CO3+D3CO2_C9_O6 → D3C19H28_O9	1.2E-12	R4
D3C96O2+D3CO2_C9_O6 → D3C18H28_O7	1.2E-12	R4
D3C89CO3+D3CO2_C9_O6 → D3C18H26_O8	1.2E-12	R4
D3C920O2+D3CO2_C9_O6 → D3C18H28_O8	1.2E-12	R4
D3C811CO3+D3CO2_C9_O6 → D3C18H26_O9	1.2E-12	R4
D3C921O2+D3CO2_C9_O6 → D3C18H28_O9	1.2E-12	R4
D3C922O2+D3CO2_C9_O6 → D3C18H28_O10	1.2E-12	R4
D3C97O2+D3CO2_C9_O6 → D3C18H28_O8	1.2E-12	R4
D3C98O2+D3CO2_C9_O6 → D3C18H28_O9	1.2E-12	R4
D3C89O2+D3CO2_C9_O6 → D3C17H26_O7	1.2E-12	R4
D3C810O2+D3CO2_C9_O6 → D3C17H26_O8	1.2E-12	R4
D3C811O2+D3CO2_C9_O6 → D3C17H26_O8	1.2E-12	R4
D3C812O2+D3CO2_C9_O6 → D3C17H26_O9	1.2E-12	R4
D3C813O2+D3CO2_C9_O6 → D3C17H26_O10	1.2E-12	R4
D3C85O2+D3CO2_C9_O6 → D3C17H26_O7	1.2E-12	R4
D3C86O2+D3CO2_C9_O6 → D3C17H26_O8	1.2E-12	R4
D3C721CO3+D3CO2_C9_O6 → D3C17H24_O9	1.2E-12	R4

D3C1O2+D3CO2_O7i1 → D3C20H32_O8	1.6E-12	R4
D3C2O2+D3CO2_O7i1 → D3C20H32_O8	1.6E-12	R4
D3C96CO3+D3CO2_O7i1 → D3C20H30_O9	1.6E-12	R4
D3CALO2+D3CO2_O7i1 → D3C20H30_O9	1.6E-12	R4
D3C106O2+D3CO2_O7i1 → D3C20H30_O10	1.6E-12	R4
D3C107O2+D3CO2_O7i1 → D3C20H30_O9	1.6E-12	R4
D3C108O2+D3CO2_O7i1 → D3C20H30_O10	1.6E-12	R4
D3C109O2+D3CO2_O7i1 → D3C20H30_O9	1.6E-12	R4
D3C920CO3+D3CO2_O7i1 → D3C20H30_O10	1.6E-12	R4
D3C96O2+D3CO2_O7i1 → D3C19H30_O8	1.6E-12	R4
D3C89CO3+D3CO2_O7i1 → D3C19H28_O9	1.6E-12	R4
D3C920O2+D3CO2_O7i1 → D3C19H30_O9	1.6E-12	R4
D3C811CO3+D3CO2_O7i1 → D3C19H28_O10	1.6E-12	R4
D3C921O2+D3CO2_O7i1 → D3C19H30_O10	1.6E-12	R4
D3C922O2+D3CO2_O7i1 → D3C19H30_O11	1.6E-12	R4
D3C97O2+D3CO2_O7i1 → D3C19H30_O9	1.6E-12	R4
D3C98O2+D3CO2_O7i1 → D3C19H30_O10	1.6E-12	R4
D3C89O2+D3CO2_O7i1 → D3C18H28_O8	1.6E-12	R4
D3C810O2+D3CO2_O7i1 → D3C18H28_O9	1.6E-12	R4
D3C811O2+D3CO2_O7i1 → D3C18H28_O9	1.6E-12	R4
D3C812O2+D3CO2_O7i1 → D3C18H28_O10	1.6E-12	R4
D3C813O2+D3CO2_O7i1 → D3C18H28_O11	1.6E-12	R4
D3C85O2+D3CO2_O7i1 → D3C18H28_O8	1.6E-12	R4
D3C86O2+D3CO2_O7i1 → D3C18H28_O9	1.6E-12	R4
D3C721CO3+D3CO2_O7i1 → D3C18H26_O10	1.6E-12	R4
D3C1O2+D3CO2_O7i2 → D3C20H32_O8	1.6E-12	R4
D3C2O2+D3CO2_O7i2 → D3C20H32_O8	1.6E-12	R4
D3C96CO3+D3CO2_O7i2 → D3C20H30_O9	1.6E-12	R4
D3CALO2+D3CO2_O7i2 → D3C20H30_O9	1.6E-12	R4
D3C106O2+D3CO2_O7i2 → D3C20H30_O10	1.6E-12	R4
D3C107O2+D3CO2_O7i2 → D3C20H30_O9	1.6E-12	R4
D3C108O2+D3CO2_O7i2 → D3C20H30_O10	1.6E-12	R4
D3C109O2+D3CO2_O7i2 → D3C20H30_O9	1.6E-12	R4
D3C920CO3+D3CO2_O7i2 → D3C20H30_O10	1.6E-12	R4
D3C96O2+D3CO2_O7i2 → D3C19H30_O8	1.6E-12	R4
D3C89CO3+D3CO2_O7i2 → D3C19H28_O9	1.6E-12	R4
D3C920O2+D3CO2_O7i2 → D3C19H30_O9	1.6E-12	R4
D3C811CO3+D3CO2_O7i2 → D3C19H28_O10	1.6E-12	R4

D3C921O2+D3CO2_O7i2 → D3C19H30_O10	1.6E-12	R4
D3C922O2+D3CO2_O7i2 → D3C19H30_O11	1.6E-12	R4
D3C97O2+D3CO2_O7i2 → D3C19H30_O9	1.6E-12	R4
D3C98O2+D3CO2_O7i2 → D3C19H30_O10	1.6E-12	R4
D3C89O2+D3CO2_O7i2 → D3C18H28_O8	1.6E-12	R4
D3C810O2+D3CO2_O7i2 → D3C18H28_O9	1.6E-12	R4
D3C811O2+D3CO2_O7i2 → D3C18H28_O9	1.6E-12	R4
D3C812O2+D3CO2_O7i2 → D3C18H28_O10	1.6E-12	R4
D3C813O2+D3CO2_O7i2 → D3C18H28_O11	1.6E-12	R4
D3C85O2+D3CO2_O7i2 → D3C18H28_O8	1.6E-12	R4
D3C86O2+D3CO2_O7i2 → D3C18H28_O9	1.6E-12	R4
D3C721CO3+D3CO2_O7i2 → D3C18H26_O10	1.6E-12	R4
D3C1O2+D3CO2_O7i3 → D3C20H32_O8	1.6E-12	R4
D3C2O2+D3CO2_O7i3 → D3C20H32_O8	1.6E-12	R4
D3C96CO3+D3CO2_O7i3 → D3C20H30_O9	1.6E-12	R4
D3CALO2+D3CO2_O7i3 → D3C20H30_O9	1.6E-12	R4
D3C106O2+D3CO2_O7i3 → D3C20H30_O10	1.6E-12	R4
D3C107O2+D3CO2_O7i3 → D3C20H30_O9	1.6E-12	R4
D3C108O2+D3CO2_O7i3 → D3C20H30_O10	1.6E-12	R4
D3C109O2+D3CO2_O7i3 → D3C20H30_O9	1.6E-12	R4
D3C920CO3+D3CO2_O7i3 → D3C20H30_O10	1.6E-12	R4
D3C96O2+D3CO2_O7i3 → D3C19H30_O8	1.6E-12	R4
D3C89CO3+D3CO2_O7i3 → D3C19H28_O9	1.6E-12	R4
D3C920O2+D3CO2_O7i3 → D3C19H30_O9	1.6E-12	R4
D3C811CO3+D3CO2_O7i3 → D3C19H28_O10	1.6E-12	R4
D3C921O2+D3CO2_O7i3 → D3C19H30_O10	1.6E-12	R4
D3C922O2+D3CO2_O7i3 → D3C19H30_O11	1.6E-12	R4
D3C97O2+D3CO2_O7i3 → D3C19H30_O9	1.6E-12	R4
D3C98O2+D3CO2_O7i3 → D3C19H30_O10	1.6E-12	R4
D3C89O2+D3CO2_O7i3 → D3C18H28_O8	1.6E-12	R4
D3C810O2+D3CO2_O7i3 → D3C18H28_O9	1.6E-12	R4
D3C811O2+D3CO2_O7i3 → D3C18H28_O9	1.6E-12	R4
D3C812O2+D3CO2_O7i3 → D3C18H28_O10	1.6E-12	R4
D3C813O2+D3CO2_O7i3 → D3C18H28_O11	1.6E-12	R4
D3C85O2+D3CO2_O7i3 → D3C18H28_O8	1.6E-12	R4
D3C86O2+D3CO2_O7i3 → D3C18H28_O9	1.6E-12	R4
D3C721CO3+D3CO2_O7i3 → D3C18H26_O10	1.6E-12	R4
D3C1O2+D3CO2_C9_O7 → D3C19H30_O8	1.6E-12	R4

D3C2O2+D3CO2_C9_O7 → D3C19H30_O8	1.6E-12	R4
D3C96CO3+D3CO2_C9_O7 → D3C19H28_O9	1.6E-12	R4
D3CALO2+D3CO2_C9_O7 → D3C19H28_O9	1.6E-12	R4
D3C106O2+D3CO2_C9_O7 → D3C19H28_O10	1.6E-12	R4
D3C107O2+D3CO2_C9_O7 → D3C19H28_O9	1.6E-12	R4
D3C108O2+D3CO2_C9_O7 → D3C19H28_O10	1.6E-12	R4
D3C109O2+D3CO2_C9_O7 → D3C19H28_O9	1.6E-12	R4
D3C920CO3+D3CO2_C9_O7 → D3C19H28_O10	1.6E-12	R4
D3C96O2+D3CO2_C9_O7 → D3C18H28_O8	1.6E-12	R4
D3C89CO3+D3CO2_C9_O7 → D3C18H28_O9	1.6E-12	R4
D3C920O2+D3CO2_C9_O7 → D3C18H28_O9	1.6E-12	R4
D3C811CO3+D3CO2_C9_O7 → D3C18H28_O10	1.6E-12	R4
D3C921O2+D3CO2_C9_O7 → D3C18H28_O10	1.6E-12	R4
D3C922O2+D3CO2_C9_O7 → D3C18H28_O11	1.6E-12	R4
D3C97O2+D3CO2_C9_O7 → D3C18H28_O9	1.6E-12	R4
D3C98O2+D3CO2_C9_O7 → D3C18H28_O10	1.6E-12	R4
D3C89O2+D3CO2_C9_O7 → D3C17H26_O8	1.6E-12	R4
D3C810O2+D3CO2_C9_O7 → D3C17H26_O9	1.6E-12	R4
D3C811O2+D3CO2_C9_O7 → D3C17H26_O9	1.6E-12	R4
D3C812O2+D3CO2_C9_O7 → D3C17H26_O10	1.6E-12	R4
D3C813O2+D3CO2_C9_O7 → D3C17H26_O11	1.6E-12	R4
D3C85O2+D3CO2_C9_O7 → D3C17H26_O8	1.6E-12	R4
D3C86O2+D3CO2_C9_O7 → D3C17H26_O9	1.6E-12	R4
D3C721CO3+D3CO2_C9_O7 → D3C17H24_O10	1.6E-12	R4
D3C1O2+D3CO2_O8i1 → D3C20H32_O9	1.6E-12	R4
D3C2O2+D3CO2_O8i1 → D3C20H32_O9	1.6E-12	R4
D3C96CO3+D3CO2_O8i1 → D3C20H30_O10	1.6E-12	R4
D3CALO2+D3CO2_O8i1 → D3C20H30_O10	1.6E-12	R4
D3C106O2+D3CO2_O8i1 → D3C20H30_O11	1.6E-12	R4
D3C107O2+D3CO2_O8i1 → D3C20H30_O10	1.6E-12	R4
D3C108O2+D3CO2_O8i1 → D3C20H30_O11	1.6E-12	R4
D3C109O2+D3CO2_O8i1 → D3C20H30_O10	1.6E-12	R4
D3C920CO3+D3CO2_O8i1 → D3C20H30_O11	1.6E-12	R4
D3C96O2+D3CO2_O8i1 → D3C19H30_O9	1.6E-12	R4
D3C89CO3+D3CO2_O8i1 → D3C19H28_O10	1.6E-12	R4
D3C920O2+D3CO2_O8i1 → D3C19H30_O10	1.6E-12	R4
D3C811CO3+D3CO2_O8i1 → D3C19H28_O11	1.6E-12	R4
D3C921O2+D3CO2_O8i1 → D3C19H30_O11	1.6E-12	R4
D3C922O2+D3CO2_O8i1 → D3C19H30_O12	1.6E-12	R4

D3C97O2+D3CO2_O8i1 → D3C19H30_O10	1.6E-12	R4
D3C98O2+D3CO2_O8i1 → D3C19H30_O11	1.6E-12	R4
D3C89O2+D3CO2_O8i1 → D3C18H28_O9	1.6E-12	R4
D3C810O2+D3CO2_O8i1 → D3C18H28_O10	1.6E-12	R4
D3C811O2+D3CO2_O8i1 → D3C18H28_O10	1.6E-12	R4
D3C812O2+D3CO2_O8i1 → D3C18H28_O11	1.6E-12	R4
D3C813O2+D3CO2_O8i1 → D3C18H28_O12	1.6E-12	R4
D3C85O2+D3CO2_O8i1 → D3C18H28_O9	1.6E-12	R4
D3C86O2+D3CO2_O8i1 → D3C18H28_O10	1.6E-12	R4
D3C721CO3+D3CO2_O8i1 → D3C18H26_O11	1.6E-12	R4
D3C1O2+D3CO2_O8i2 → D3C20H32_O9	1.6E-12	R4
D3C2O2+D3CO2_O8i2 → D3C20H32_O9	1.6E-12	R4
D3C96CO3+D3CO2_O8i2 → D3C20H30_O10	1.6E-12	R4
D3CALO2+D3CO2_O8i2 → D3C20H30_O10	1.6E-12	R4
D3C106O2+D3CO2_O8i2 → D3C20H30_O11	1.6E-12	R4
D3C107O2+D3CO2_O8i2 → D3C20H30_O10	1.6E-12	R4
D3C108O2+D3CO2_O8i2 → D3C20H30_O11	1.6E-12	R4
D3C109O2+D3CO2_O8i2 → D3C20H30_O10	1.6E-12	R4
D3C920CO3+D3CO2_O8i2 → D3C20H30_O11	1.6E-12	R4
D3C96O2+D3CO2_O8i2 → D3C19H30_O9	1.6E-12	R4
D3C89CO3+D3CO2_O8i2 → D3C19H28_O10	1.6E-12	R4
D3C920O2+D3CO2_O8i2 → D3C19H30_O10	1.6E-12	R4
D3C811CO3+D3CO2_O8i2 → D3C19H28_O11	1.6E-12	R4
D3C921O2+D3CO2_O8i2 → D3C19H30_O11	1.6E-12	R4
D3C922O2+D3CO2_O8i2 → D3C19H30_O12	1.6E-12	R4
D3C97O2+D3CO2_O8i2 → D3C19H30_O10	1.6E-12	R4
D3C98O2+D3CO2_O8i2 → D3C19H30_O11	1.6E-12	R4
D3C89O2+D3CO2_O8i2 → D3C18H28_O9	1.6E-12	R4
D3C810O2+D3CO2_O8i2 → D3C18H28_O10	1.6E-12	R4
D3C811O2+D3CO2_O8i2 → D3C18H28_O10	1.6E-12	R4
D3C812O2+D3CO2_O8i2 → D3C18H28_O11	1.6E-12	R4
D3C813O2+D3CO2_O8i2 → D3C18H28_O12	1.6E-12	R4
D3C85O2+D3CO2_O8i2 → D3C18H28_O9	1.6E-12	R4
D3C86O2+D3CO2_O8i2 → D3C18H28_O10	1.6E-12	R4
D3C721CO3+D3CO2_O8i2 → D3C18H26_O11	1.6E-12	R4
D3C1O2+D3CO2_O8i3 → D3C20H32_O9	1.6E-12	R4
D3C2O2+D3CO2_O8i3 → D3C20H32_O9	1.6E-12	R4
D3C96CO3+D3CO2_O8i3 → D3C20H30_O10	1.6E-12	R4

D3CALO2+D3CO2_O8i3 → D3C20H30_O10	1.6E-12	R4
D3C106O2+D3CO2_O8i3 → D3C20H30_O11	1.6E-12	R4
D3C107O2+D3CO2_O8i3 → D3C20H30_O10	1.6E-12	R4
D3C108O2+D3CO2_O8i3 → D3C20H30_O11	1.6E-12	R4
D3C109O2+D3CO2_O8i3 → D3C20H30_O10	1.6E-12	R4
D3C920CO3+D3CO2_O8i3 → D3C20H30_O11	1.6E-12	R4
D3C96O2+D3CO2_O8i3 → D3C19H30_O9	1.6E-12	R4
D3C89CO3+D3CO2_O8i3 → D3C19H28_O10	1.6E-12	R4
D3C920O2+D3CO2_O8i3 → D3C19H30_O10	1.6E-12	R4
D3C811CO3+D3CO2_O8i3 → D3C19H28_O11	1.6E-12	R4
D3C921O2+D3CO2_O8i3 → D3C19H30_O11	1.6E-12	R4
D3C922O2+D3CO2_O8i3 → D3C19H30_O12	1.6E-12	R4
D3C97O2+D3CO2_O8i3 → D3C19H30_O10	1.6E-12	R4
D3C98O2+D3CO2_O8i3 → D3C19H30_O11	1.6E-12	R4
D3C89O2+D3CO2_O8i3 → D3C18H28_O9	1.6E-12	R4
D3C810O2+D3CO2_O8i3 → D3C18H28_O10	1.6E-12	R4
D3C811O2+D3CO2_O8i3 → D3C18H28_O10	1.6E-12	R4
D3C812O2+D3CO2_O8i3 → D3C18H28_O11	1.6E-12	R4
D3C813O2+D3CO2_O8i3 → D3C18H28_O12	1.6E-12	R4
D3C85O2+D3CO2_O8i3 → D3C18H28_O9	1.6E-12	R4
D3C86O2+D3CO2_O8i3 → D3C18H28_O10	1.6E-12	R4
D3C721CO3+D3CO2_O8i3 → D3C18H26_O11	1.6E-12	R4
D3C1O2+D3CO2_C9_O8 → D3C19H30_O9	1.6E-12	R4
D3C2O2+D3CO2_C9_O8 → D3C19H30_O9	1.6E-12	R4
D3C96CO3+D3CO2_C9_O8 → D3C19H28_O10	1.6E-12	R4
D3CALO2+D3CO2_C9_O8 → D3C19H28_O10	1.6E-12	R4
D3C106O2+D3CO2_C9_O8 → D3C19H28_O11	1.6E-12	R4
D3C107O2+D3CO2_C9_O8 → D3C19H28_O10	1.6E-12	R4
D3C108O2+D3CO2_C9_O8 → D3C19H28_O11	1.6E-12	R4
D3C109O2+D3CO2_C9_O8 → D3C19H28_O10	1.6E-12	R4
D3C920CO3+D3CO2_C9_O8 → D3C19H28_O11	1.6E-12	R4
D3C96O2+D3CO2_C9_O8 → D3C18H28_O9	1.6E-12	R4
D3C89CO3+D3CO2_C9_O8 → D3C18H26_O10	1.6E-12	R4
D3C920O2+D3CO2_C9_O8 → D3C18H28_O10	1.6E-12	R4
D3C811CO3+D3CO2_C9_O8 → D3C18H26_O11	1.6E-12	R4
D3C921O2+D3CO2_C9_O8 → D3C18H28_O11	1.6E-12	R4
D3C922O2+D3CO2_C9_O8 → D3C18H28_O12	1.6E-12	R4
D3C97O2+D3CO2_C9_O8 → D3C18H28_O10	1.6E-12	R4
D3C98O2+D3CO2_C9_O8 → D3C18H28_O11	1.6E-12	R4

D3C89O2+D3CO2_C9_O8 → D3C17H26_O9	1.6E-12	R4
D3C810O2+D3CO2_C9_O8 → D3C17H26_O10	1.6E-12	R4
D3C811O2+D3CO2_C9_O8 → D3C17H26_O10	1.6E-12	R4
D3C812O2+D3CO2_C9_O8 → D3C17H26_O11	1.6E-12	R4
D3C813O2+D3CO2_C9_O8 → D3C17H26_O12	1.6E-12	R4
D3C85O2+D3CO2_C9_O8 → D3C17H26_O9	1.6E-12	R4
D3C86O2+D3CO2_C9_O8 → D3C17H26_O10	1.6E-12	R4
D3C721CO3+D3CO2_C9_O8 → D3C17H24_O11	1.6E-12	R4
D3C1O2+D3CO2_O9i1 → D3C20H32_O10	1.6E-12	R4
D3C2O2+D3CO2_O9i1 → D3C20H32_O10	1.6E-12	R4
D3C96CO3+D3CO2_O9i1 → D3C20H30_O11	1.6E-12	R4
D3CALO2+D3CO2_O9i1 → D3C20H30_O11	1.6E-12	R4
D3C106O2+D3CO2_O9i1 → D3C20H30_O12	1.6E-12	R4
D3C107O2+D3CO2_O9i1 → D3C20H30_O11	1.6E-12	R4
D3C108O2+D3CO2_O9i1 → D3C20H30_O12	1.6E-12	R4
D3C109O2+D3CO2_O9i1 → D3C20H30_O11	1.6E-12	R4
D3C920CO3+D3CO2_O9i1 → D3C20H30_O12	1.6E-12	R4
D3C96O2+D3CO2_O9i1 → D3C19H30_O10	1.6E-12	R4
D3C89CO3+D3CO2_O9i1 → D3C19H28_O11	1.6E-12	R4
D3C920O2+D3CO2_O9i1 → D3C19H30_O11	1.6E-12	R4
D3C811CO3+D3CO2_O9i1 → D3C19H28_O12	1.6E-12	R4
D3C921O2+D3CO2_O9i1 → D3C19H30_O12	1.6E-12	R4
D3C922O2+D3CO2_O9i1 → D3C19H30_O13	1.6E-12	R4
D3C97O2+D3CO2_O9i1 → D3C19H30_O11	1.6E-12	R4
D3C98O2+D3CO2_O9i1 → D3C19H30_O12	1.6E-12	R4
D3C89O2+D3CO2_O9i1 → D3C18H28_O10	1.6E-12	R4
D3C810O2+D3CO2_O9i1 → D3C18H28_O11	1.6E-12	R4
D3C811O2+D3CO2_O9i1 → D3C18H28_O11	1.6E-12	R4
D3C812O2+D3CO2_O9i1 → D3C18H28_O12	1.6E-12	R4
D3C813O2+D3CO2_O9i1 → D3C18H28_O13	1.6E-12	R4
D3C85O2+D3CO2_O9i1 → D3C18H28_O10	1.6E-12	R4
D3C86O2+D3CO2_O9i1 → D3C18H28_O11	1.6E-12	R4
D3C721CO3+D3CO2_O9i1 → D3C18H26_O12	1.6E-12	R4
D3C1O2+D3CO2_O9i2 → D3C20H32_O10	1.6E-12	R4
D3C2O2+D3CO2_O9i2 → D3C20H32_O10	1.6E-12	R4
D3C96CO3+D3CO2_O9i2 → D3C20H30_O11	1.6E-12	R4
D3CALO2+D3CO2_O9i2 → D3C20H30_O11	1.6E-12	R4
D3C106O2+D3CO2_O9i2 → D3C20H30_O12	1.6E-12	R4

D3C107O2+D3CO2_O9i2 → D3C20H30_O11	1.6E-12	R4
D3C108O2+D3CO2_O9i2 → D3C20H30_O12	1.6E-12	R4
D3C109O2+D3CO2_O9i2 → D3C20H30_O11	1.6E-12	R4
D3C920CO3+D3CO2_O9i2 → D3C20H30_O12	1.6E-12	R4
D3C96O2+D3CO2_O9i2 → D3C19H30_O10	1.6E-12	R4
D3C89CO3+D3CO2_O9i2 → D3C19H28_O11	1.6E-12	R4
D3C920O2+D3CO2_O9i2 → D3C19H30_O11	1.6E-12	R4
D3C811CO3+D3CO2_O9i2 → D3C19H28_O12	1.6E-12	R4
D3C921O2+D3CO2_O9i2 → D3C19H30_O12	1.6E-12	R4
D3C922O2+D3CO2_O9i2 → D3C19H30_O13	1.6E-12	R4
D3C97O2+D3CO2_O9i2 → D3C19H30_O11	1.6E-12	R4
D3C98O2+D3CO2_O9i2 → D3C19H30_O12	1.6E-12	R4
D3C89O2+D3CO2_O9i2 → D3C18H28_O10	1.6E-12	R4
D3C810O2+D3CO2_O9i2 → D3C18H28_O11	1.6E-12	R4
D3C811O2+D3CO2_O9i2 → D3C18H28_O11	1.6E-12	R4
D3C812O2+D3CO2_O9i2 → D3C18H28_O12	1.6E-12	R4
D3C813O2+D3CO2_O9i2 → D3C18H28_O13	1.6E-12	R4
D3C85O2+D3CO2_O9i2 → D3C18H28_O10	1.6E-12	R4
D3C86O2+D3CO2_O9i2 → D3C18H28_O11	1.6E-12	R4
D3C721CO3+D3CO2_O9i2 → D3C18H26_O12	1.6E-12	R4
D3C1O2+D3CO2_O9i3 → D3C20H32_O10	1.6E-12	R4
D3C2O2+D3CO2_O9i3 → D3C20H32_O10	1.6E-12	R4
D3C96CO3+D3CO2_O9i3 → D3C20H30_O11	1.6E-12	R4
D3CALO2+D3CO2_O9i3 → D3C20H30_O11	1.6E-12	R4
D3C106O2+D3CO2_O9i3 → D3C20H30_O12	1.6E-12	R4
D3C107O2+D3CO2_O9i3 → D3C20H30_O11	1.6E-12	R4
D3C108O2+D3CO2_O9i3 → D3C20H30_O12	1.6E-12	R4
D3C109O2+D3CO2_O9i3 → D3C20H30_O11	1.6E-12	R4
D3C920CO3+D3CO2_O9i3 → D3C20H30_O12	1.6E-12	R4
D3C96O2+D3CO2_O9i3 → D3C19H30_O10	1.6E-12	R4
D3C89CO3+D3CO2_O9i3 → D3C19H28_O11	1.6E-12	R4
D3C920O2+D3CO2_O9i3 → D3C19H30_O11	1.6E-12	R4
D3C811CO3+D3CO2_O9i3 → D3C19H28_O12	1.6E-12	R4
D3C921O2+D3CO2_O9i3 → D3C19H30_O12	1.6E-12	R4
D3C922O2+D3CO2_O9i3 → D3C19H30_O13	1.6E-12	R4
D3C97O2+D3CO2_O9i3 → D3C19H30_O11	1.6E-12	R4
D3C98O2+D3CO2_O9i3 → D3C19H30_O12	1.6E-12	R4
D3C89O2+D3CO2_O9i3 → D3C18H28_O10	1.6E-12	R4
D3C810O2+D3CO2_O9i3 → D3C18H28_O11	1.6E-12	R4

D3C811O2+D3CO2_O9i3 → D3C18H28_O11	1.6E-12	R4
D3C812O2+D3CO2_O9i3 → D3C18H28_O12	1.6E-12	R4
D3C813O2+D3CO2_O9i3 → D3C18H28_O13	1.6E-12	R4
D3C85O2+D3CO2_O9i3 → D3C18H28_O10	1.6E-12	R4
D3C86O2+D3CO2_O9i3 → D3C18H28_O11	1.6E-12	R4
D3C721CO3+D3CO2_O9i3 → D3C18H26_O12	1.6E-12	R4
D3C1O2+D3CO2_C9_O9 → D3C19H30_O10	1.6E-12	R4
D3C2O2+D3CO2_C9_O9 → D3C19H30_O10	1.6E-12	R4
D3C96CO3+D3CO2_C9_O9 → D3C19H28_O11	1.6E-12	R4
D3CALO2+D3CO2_C9_O9 → D3C19H28_O11	1.6E-12	R4
D3C106O2+D3CO2_C9_O9 → D3C19H28_O12	1.6E-12	R4
D3C107O2+D3CO2_C9_O9 → D3C19H28_O11	1.6E-12	R4
D3C108O2+D3CO2_C9_O9 → D3C19H28_O12	1.6E-12	R4
D3C109O2+D3CO2_C9_O9 → D3C19H28_O11	1.6E-12	R4
D3C920CO3+D3CO2_C9_O9 → D3C19H28_O12	1.6E-12	R4
D3C96O2+D3CO2_C9_O9 → D3C18H28_O10	1.6E-12	R4
D3C89CO3+D3CO2_C9_O9 → D3C18H26_O11	1.6E-12	R4
D3C920O2+D3CO2_C9_O9 → D3C18H28_O11	1.6E-12	R4
D3C811CO3+D3CO2_C9_O9 → D3C18H26_O12	1.6E-12	R4
D3C921O2+D3CO2_C9_O9 → D3C18H28_O12	1.6E-12	R4
D3C922O2+D3CO2_C9_O9 → D3C18H28_O13	1.6E-12	R4
D3C97O2+D3CO2_C9_O9 → D3C18H28_O11	1.6E-12	R4
D3C98O2+D3CO2_C9_O9 → D3C18H28_O12	1.6E-12	R4
D3C89O2+D3CO2_C9_O9 → D3C17H26_O10	1.6E-12	R4
D3C810O2+D3CO2_C9_O9 → D3C17H26_O11	1.6E-12	R4
D3C811O2+D3CO2_C9_O9 → D3C17H26_O11	1.6E-12	R4
D3C812O2+D3CO2_C9_O9 → D3C17H26_O12	1.6E-12	R4
D3C813O2+D3CO2_C9_O9 → D3C17H26_O13	1.6E-12	R4
D3C85O2+D3CO2_C9_O9 → D3C17H26_O10	1.6E-12	R4
D3C86O2+D3CO2_C9_O9 → D3C17H26_O11	1.6E-12	R4
D3C721CO3+D3CO2_C9_O9 → D3C17H24_O13	1.6E-12	R4
D3C1O2+D3CO2_O10i1 → D3C20H32_O11	1.6E-12	R4
D3C2O2+D3CO2_O10i1 → D3C20H32_O11	1.6E-12	R4
D3C96CO3+D3CO2_O10i1 → D3C20H30_O12	1.6E-12	R4
D3CALO2+D3CO2_O10i1 → D3C20H30_O12	1.6E-12	R4
D3C106O2+D3CO2_O10i1 → D3C20H30_O13	1.6E-12	R4
D3C107O2+D3CO2_O10i1 → D3C20H30_O12	1.6E-12	R4
D3C108O2+D3CO2_O10i1 → D3C20H30_O13	1.6E-12	R4

D3C109O2+D3CO2_O10i1 → D3C20H30_O12	1.6E-12	R4
D3C920CO3+D3CO2_O10i1 → D3C20H30_O13	1.6E-12	R4
D3C96O2+D3CO2_O10i1 → D3C19H30_O11	1.6E-12	R4
D3C89CO3+D3CO2_O10i1 → D3C19H28_O12	1.6E-12	R4
D3C920O2+D3CO2_O10i1 → D3C19H30_O12	1.6E-12	R4
D3C811CO3+D3CO2_O10i1 → D3C19H28_O13	1.6E-12	R4
D3C921O2+D3CO2_O10i1 → D3C19H30_O13	1.6E-12	R4
D3C922O2+D3CO2_O10i1 → D3C19H30_O14	1.6E-12	R4
D3C97O2+D3CO2_O10i1 → D3C19H30_O12	1.6E-12	R4
D3C98O2+D3CO2_O10i1 → D3C19H30_O13	1.6E-12	R4
D3C89O2+D3CO2_O10i1 → D3C18H28_O11	1.6E-12	R4
D3C810O2+D3CO2_O10i1 → D3C18H28_O12	1.6E-12	R4
D3C811O2+D3CO2_O10i1 → D3C18H28_O12	1.6E-12	R4
D3C812O2+D3CO2_O10i1 → D3C18H28_O13	1.6E-12	R4
D3C813O2+D3CO2_O10i1 → D3C18H28_O14	1.6E-12	R4
D3C85O2+D3CO2_O10i1 → D3C18H28_O11	1.6E-12	R4
D3C86O2+D3CO2_O10i1 → D3C18H28_O12	1.6E-12	R4
D3C721CO3+D3CO2_O10i1 → D3C18H26_O13	1.6E-12	R4
D3C1O2+D3CO2_O10i3 → D3C20H32_O11	1.6E-12	R4
D3C2O2+D3CO2_O10i3 → D3C20H32_O11	1.6E-12	R4
D3C96CO3+D3CO2_O10i3 → D3C20H30_O12	1.6E-12	R4
D3CALO2+D3CO2_O10i3 → D3C20H30_O12	1.6E-12	R4
D3C106O2+D3CO2_O10i3 → D3C20H30_O13	1.6E-12	R4
D3C107O2+D3CO2_O10i3 → D3C20H30_O12	1.6E-12	R4
D3C108O2+D3CO2_O10i3 → D3C20H30_O13	1.6E-12	R4
D3C109O2+D3CO2_O10i3 → D3C20H30_O12	1.6E-12	R4
D3C920CO3+D3CO2_O10i3 → D3C20H30_O13	1.6E-12	R4
D3C96O2+D3CO2_O10i3 → D3C19H30_O11	1.6E-12	R4
D3C89CO3+D3CO2_O10i3 → D3C19H28_O12	1.6E-12	R4
D3C920O2+D3CO2_O10i3 → D3C19H30_O12	1.6E-12	R4
D3C811CO3+D3CO2_O10i3 → D3C19H28_O13	1.6E-12	R4
D3C921O2+D3CO2_O10i3 → D3C19H30_O13	1.6E-12	R4
D3C922O2+D3CO2_O10i3 → D3C19H30_O14	1.6E-12	R4
D3C97O2+D3CO2_O10i3 → D3C19H30_O12	1.6E-12	R4
D3C98O2+D3CO2_O10i3 → D3C19H30_O13	1.6E-12	R4
D3C89O2+D3CO2_O10i3 → D3C18H28_O11	1.6E-12	R4
D3C810O2+D3CO2_O10i3 → D3C18H28_O12	1.6E-12	R4
D3C811O2+D3CO2_O10i3 → D3C18H28_O12	1.6E-12	R4
D3C812O2+D3CO2_O10i3 → D3C18H28_O13	1.6E-12	R4

D3C813O2+D3CO2_O10i3 → D3C18H28_O14	1.6E-12	R4
D3C85O2+D3CO2_O10i3 → D3C18H28_O11	1.6E-12	R4
D3C86O2+D3CO2_O10i3 → D3C18H28_O12	1.6E-12	R4
D3C721CO3+D3CO2_O10i3 → D3C18H26_O13	1.6E-12	R4
D3C1O2+D3CO2_C9_O10 → D3C19H30_O11	1.6E-12	R4
D3C2O2+D3CO2_C9_O10 → D3C19H30_O11	1.6E-12	R4
D3C96CO3+D3CO2_C9_O10 → D3C19H28_O12	1.6E-12	R4
D3CALO2+D3CO2_C9_O10 → D3C19H28_O12	1.6E-12	R4
D3C106O2+D3CO2_C9_O10 → D3C19H28_O13	1.6E-12	R4
D3C107O2+D3CO2_C9_O10 → D3C19H28_O12	1.6E-12	R4
D3C108O2+D3CO2_C9_O10 → D3C19H28_O13	1.6E-12	R4
D3C109O2+D3CO2_C9_O10 → D3C19H28_O12	1.6E-12	R4
D3C920CO3+D3CO2_C9_O10 → D3C19H28_O13	1.6E-12	R4
D3C96O2+D3CO2_C9_O10 → D3C18H28_O11	1.6E-12	R4
D3C89CO3+D3CO2_C9_O10 → D3C18H26_O12	1.6E-12	R4
D3C920O2+D3CO2_C9_O10 → D3C18H28_O12	1.6E-12	R4
D3C811CO3+D3CO2_C9_O10 → D3C18H26_O13	1.6E-12	R4
D3C921O2+D3CO2_C9_O10 → D3C18H28_O13	1.6E-12	R4
D3C922O2+D3CO2_C9_O10 → D3C18H28_O14	1.6E-12	R4
D3C97O2+D3CO2_C9_O10 → D3C18H28_O12	1.6E-12	R4
D3C98O2+D3CO2_C9_O10 → D3C18H28_O13	1.6E-12	R4
D3C89O2+D3CO2_C9_O10 → D3C17H26_O11	1.6E-12	R4
D3C810O2+D3CO2_C9_O10 → D3C17H26_O12	1.6E-12	R4
D3C811O2+D3CO2_C9_O10 → D3C17H26_O12	1.6E-12	R4
D3C812O2+D3CO2_C9_O10 → D3C17H26_O13	1.6E-12	R4
D3C813O2+D3CO2_C9_O10 → D3C17H26_O14	1.6E-12	R4
D3C85O2+D3CO2_C9_O10 → D3C17H26_O11	1.6E-12	R4
D3C86O2+D3CO2_C9_O10 → D3C17H26_O12	1.6E-12	R4
D3C721CO3+D3CO2_C9_O10 → D3C17H24_O14	1.6E-12	R4
D3C1O2+D3CO2_O11i1 → D3C20H32_O12	1.6E-12	R4
D3C2O2+D3CO2_O11i1 → D3C20H32_O12	1.6E-12	R4
D3C96CO3+D3CO2_O11i1 → D3C20H30_O13	1.6E-12	R4
D3CALO2+D3CO2_O11i1 → D3C20H30_O13	1.6E-12	R4
D3C106O2+D3CO2_O11i1 → D3C20H30_O14	1.6E-12	R4
D3C107O2+D3CO2_O11i1 → D3C20H30_O13	1.6E-12	R4
D3C108O2+D3CO2_O11i1 → D3C20H30_O14	1.6E-12	R4
D3C109O2+D3CO2_O11i1 → D3C20H30_O13	1.6E-12	R4
D3C920CO3+D3CO2_O11i1 → D3C20H30_O14	1.6E-12	R4

D3C96O2+D3CO2_O11i1 → D3C19H30_O12	1.6E-12	R4
D3C89CO3+D3CO2_O11i1 → D3C19H28_O13	1.6E-12	R4
D3C920O2+D3CO2_O11i1 → D3C19H30_O13	1.6E-12	R4
D3C811CO3+D3CO2_O11i1 → D3C19H28_O14	1.6E-12	R4
D3C921O2+D3CO2_O11i1 → D3C19H30_O14	1.6E-12	R4
D3C922O2+D3CO2_O11i1 → D3C19H30_O15	1.6E-12	R4
D3C97O2+D3CO2_O11i1 → D3C19H30_O13	1.6E-12	R4
D3C98O2+D3CO2_O11i1 → D3C19H30_O14	1.6E-12	R4
D3C89O2+D3CO2_O11i1 → D3C18H28_O12	1.6E-12	R4
D3C810O2+D3CO2_O11i1 → D3C18H28_O13	1.6E-12	R4
D3C811O2+D3CO2_O11i1 → D3C18H28_O13	1.6E-12	R4
D3C812O2+D3CO2_O11i1 → D3C18H28_O14	1.6E-12	R4
D3C813O2+D3CO2_O11i1 → D3C18H28_O15	1.6E-12	R4
D3C85O2+D3CO2_O11i1 → D3C18H28_O12	1.6E-12	R4
D3C86O2+D3CO2_O11i1 → D3C18H28_O13	1.6E-12	R4
D3C721CO3+D3CO2_O11i1 → D3C18H26_O14	1.6E-12	R4
D3C1O2+D3CO2_O11i2 → D3C20H32_O12	1.6E-12	R4
D3C2O2+D3CO2_O11i2 → D3C20H32_O12	1.6E-12	R4
D3C96CO3+D3CO2_O11i2 → D3C20H30_O13	1.6E-12	R4
D3CALO2+D3CO2_O11i2 → D3C20H30_O13	1.6E-12	R4
D3C106O2+D3CO2_O11i2 → D3C20H30_O14	1.6E-12	R4
D3C107O2+D3CO2_O11i2 → D3C20H30_O13	1.6E-12	R4
D3C108O2+D3CO2_O11i2 → D3C20H30_O14	1.6E-12	R4
D3C109O2+D3CO2_O11i2 → D3C20H30_O13	1.6E-12	R4
D3C920CO3+D3CO2_O11i2 → D3C20H30_O14	1.6E-12	R4
D3C96O2+D3CO2_O11i2 → D3C19H30_O12	1.6E-12	R4
D3C89CO3+D3CO2_O11i2 → D3C19H28_O13	1.6E-12	R4
D3C920O2+D3CO2_O11i2 → D3C19H30_O13	1.6E-12	R4
D3C811CO3+D3CO2_O11i2 → D3C19H28_O14	1.6E-12	R4
D3C921O2+D3CO2_O11i2 → D3C19H30_O14	1.6E-12	R4
D3C922O2+D3CO2_O11i2 → D3C19H30_O15	1.6E-12	R4
D3C97O2+D3CO2_O11i2 → D3C19H30_O13	1.6E-12	R4
D3C98O2+D3CO2_O11i2 → D3C19H30_O14	1.6E-12	R4
D3C89O2+D3CO2_O11i2 → D3C18H28_O12	1.6E-12	R4
D3C810O2+D3CO2_O11i2 → D3C18H28_O13	1.6E-12	R4
D3C811O2+D3CO2_O11i2 → D3C18H28_O13	1.6E-12	R4
D3C812O2+D3CO2_O11i2 → D3C18H28_O14	1.6E-12	R4
D3C813O2+D3CO2_O11i2 → D3C18H28_O15	1.6E-12	R4
D3C85O2+D3CO2_O11i2 → D3C18H28_O12	1.6E-12	R4

D3C86O2+D3CO2_O11i2 → D3C18H28_O13	1.6E-12	R4
D3C721CO3+D3CO2_O11i2 → D3C18H26_O14	1.6E-12	R4
D3C1O2+D3CO2_O12 → D3C20H32_O13	1.6E-12	R4
D3C2O2+D3CO2_O12 → D3C20H32_O13	1.6E-12	R4
D3C96CO3+D3CO2_O12 → D3C20H30_O14	1.6E-12	R4
D3CALO2+D3CO2_O12 → D3C20H30_O14	1.6E-12	R4
D3C106O2+D3CO2_O12 → D3C20H30_O15	1.6E-12	R4
D3C107O2+D3CO2_O12 → D3C20H30_O14	1.6E-12	R4
D3C108O2+D3CO2_O12 → D3C20H30_O15	1.6E-12	R4
D3C109O2+D3CO2_O12 → D3C20H30_O14	1.6E-12	R4
D3C920CO3+D3CO2_O12 → D3C20H30_O15	1.6E-12	R4
D3C96O2+D3CO2_O12 → D3C19H30_O13	1.6E-12	R4
D3C89CO3+D3CO2_O12 → D3C19H28_O14	1.6E-12	R4
D3C920O2+D3CO2_O12 → D3C19H30_O14	1.6E-12	R4
D3C811CO3+D3CO2_O12 → D3C19H28_O15	1.6E-12	R4
D3C921O2+D3CO2_O12 → D3C19H30_O15	1.6E-12	R4
D3C922O2+D3CO2_O12 → D3C19H30_O16	1.6E-12	R4
D3C97O2+D3CO2_O12 → D3C19H30_O14	1.6E-12	R4
D3C98O2+D3CO2_O12 → D3C19H30_O15	1.6E-12	R4
D3C89O2+D3CO2_O12 → D3C18H28_O13	1.6E-12	R4
D3C810O2+D3CO2_O12 → D3C18H28_O14	1.6E-12	R4
D3C811O2+D3CO2_O12 → D3C18H28_O14	1.6E-12	R4
D3C812O2+D3CO2_O12 → D3C18H28_O15	1.6E-12	R4
D3C813O2+D3CO2_O12 → D3C18H28_O16	1.6E-12	R4
D3C85O2+D3CO2_O12 → D3C18H28_O13	1.6E-12	R4
D3C86O2+D3CO2_O12 → D3C18H28_O14	1.6E-12	R4
D3C721CO3+D3CO2_O12 → D3C18H26_O15	1.6E-12	R4

References

Chen, H., Ren, Y., Cazaunau, M., Daële, V., Hu, Y., Chen, J., and Mellouki, A.: Rate coefficients for the reaction of ozone with 2- and 3-carene, Chemical Physics Letters, 621, 71-77, 10.1016/j.cplett.2014.12.056, 2015.

DeCarlo, P. F., Kimmel, J. R., Trimborn, A., Northway, M. J., Jayne, J. T., Aiken, A. C., Gonin, M., Fuhrer, K., Horvath, T., Docherty, K. S., Worsnop, D. R., and Jimenez, J. L.: Field-Deployable, High-Resolution, Time-of-Flight Aerosol Mass Spectrometer, Analytical Chemistry, 78, 8281-8289, 10.1021/ac061249n, 2006.

Dillon, T. J., Dulitz, K., Groß, C. B. M., and Crowley, J. N.: Temperature-dependent rate coefficients for the reactions of the hydroxyl radical with the atmospheric biogenics isoprene, alpha-pinene and delta-3-carene, Atmospheric Chemistry and Physics, 17, 15137-15150, 10.5194/acp-17-15137-2017, 2017.

Ehn, M., Thornton, J. A., Kleist, E., Sipilä, M., Junninen, H., Pullinen, I., Springer, M., Rubach, F., Tillmann, R., and Lee, B.: A large source of low-volatility secondary organic aerosol, Nature, 506, 476-479, 2014.

Eiguren-Fernandez, A., Lewis, G. S., Spielman, S. R., and Hering, S. V.: Time-resolved characterization of particle associated polycyclic aromatic hydrocarbons using a newly-developed sequential spot sampler with automated extraction and analysis, Atmospheric Environment, 96, 125-134, https://doi.org/10.1016/j.atmosenv.2014.07.031, 2014.

Eiguren Fernandez, A., Lewis, G. S., and Hering, S. V.: Design and Laboratory Evaluation of a Sequential Spot Sampler for Time-Resolved Measurement of Airborne Particle Composition, Aerosol Science and Technology, 48, 655-663, 10.1080/02786826.2014.911409, 2014.

Hantschke, L., Novelli, A., Bohn, B., Cho, C., Reimer, D., Rohrer, F., Tillmann, R., Glowania, M., Hofzumahaus, A., Kiendler-Scharr, A., Wahner, A., and Fuchs, H.: Atmospheric photooxidation and ozonolysis of Δ3-carene and 3-caronaldehyde: rate constants and product yields, Atmospheric Chemistry and Physics, 21, 12665-12685, 10.5194/acp-21-12665-2021, 2021.

Jokinen, T., Sipilä, M., Junninen, H., Ehn, M., Lönn, G., Hakala, J., Petäjä, T., Mauldin, R. L., Kulmala, M., and Worsnop, D. R.: Atmospheric sulphuric acid and neutral cluster measurements using CI-APi-TOF, Atmospheric Chemistry and Physics, 12, 4117-4125, 10.5194/acp-12-4117-2012, 2012.

Jordan, A., Haidacher, S., Hanel, G., Hartungen, E., Märk, L., Seehauser, H., Schottkowsky, R., Sulzer, P., and Märk, T. D.: A high resolution and high sensitivity proton-transfer-reaction time-of-flight mass spectrometer (PTR-TOF-MS), International Journal of Mass Spectrometry, 286, 122-128, 10.1016/j.ijms.2009.07.005, 2009.

Kristensen, K., Jensen, L., Glasius, M., and Bilde, M.: The effect of sub-zero temperature on the formation and composition of secondary organic aerosol from ozonolysis of alpha-pinene, Environmental Science: Processes & Impacts, 19, 1220-1234, 2017.

Li, L., Thomsen, D., Wu, C., Priestley, M., Iversen, E. M., Tygesen Skønager, J., Luo, Y., Ehn, M., Roldin, P., Pedersen, H. B., Bilde, M., Glasius, M., and Hallquist, M.: Gas-to-Particle Partitioning of Products from Ozonolysis of Δ^3-Carene and the Effect of Temperature and Relative Humidity, The Journal of Physical Chemistry A, 128, 918-928, 10.1021/acs.jpca.3c07316, 2024.

Lopez-Hilfiker, F. D., Mohr, C., Ehn, M., Rubach, F., Kleist, E., Wildt, J., Mentel, T. F., Lutz, A., Hallquist, M., Worsnop, D., and Thornton, J. A.: A novel method for online analysis of gas and particle composition: description and evaluation of a Filter Inlet for Gases and AEROsols (FIGAERO), Atmospheric Measurement Techniques, 7, 983-1001, 10.5194/amt-7-983-2014, 2014.

Peräkylä, O., Riva, M., Heikkinen, L., Quéléver, L., Roldin, P., and Ehn, M.: Experimental investigation into the volatilities of highly oxygenated organic molecules (HOMs), Atmospheric Chemistry and Phyics, 20, 649-669, 10.5194/acp-20-649-2020, 2020.

Quéléver, L. L. J., Kristensen, K., Normann Jensen, L., Rosati, B., Teiwes, R., Daellenbach, K. R., Peräkylä, O., Roldin, P., Bossi, R., Pedersen, H. B., Glasius, M., Bilde, M., and Ehn, M.: Effect of temperature on the formation of highly oxygenated organic molecules (HOMs) from alpha-pinene ozonolysis, Atmospheric Chemistry and Physics, 19, 7609-7625, 10.5194/acp-19-7609-2019, 2019.

Riva, M., Rantala, P., Krechmer, J. E., Peräkylä, O., Zhang, Y., Heikkinen, L., Garmash, O., Yan, C., Kulmala, M., Worsnop, D., and Ehn, M.: Evaluating the performance of five different chemical ionization techniques for detecting gaseous oxygenated organic species, Atmospheric Measurement Techniques, 12, 2403-2421, 10.5194/amt-12-2403-2019, 2019.

Thomsen, D., Iversen, E. M., Skønager, J. T., Luo, Y., Li, L., Roldin, P., Priestley, M., Pedersen, H. B., Hallquist, M., and Ehn, M.: The effect of temperature and relative humidity on secondary organic aerosol formation from ozonolysis of Δ^3-carene, Environmental Science: Atmospheres, 4, 88-103, 2024.

Tuovinen, S., Kontkanen, J., Cai, R., and Kulmala, M.: Condensation sink of atmospheric vapors: the effect of vapor properties and the resulting uncertainties, Environmental Science: Atmospheres, 1, 543-557, 2021.

Wang, L., Liu, Y., and Wang, L.: Ozonolysis of 3-carene in the atmosphere. Formation mechanism of hydroxyl radical and secondary ozonides, Physical Chemistry Chemical Physics, 21, 8081-8091, 10.1039/c8cp07195k, 2019.